

A Proposal for the Paul Scherrer Institute π M1 beam line

Studying the Proton “Radius” Puzzle with μp Elastic Scattering The MUon proton Scattering Experiment (MUSE) Collaboration^a

R. Gilman (Contact person),¹ E.J. Downie (Spokesperson),² G. Ron (Spokesperson),³
A. Afanasev,² J. Arrington,⁴ O. Ates,⁵ F. Benmokhtar,⁶ J. Bernauer,⁷ E. Brash,⁸ W. J. Briscoe,²
K. Deiters,⁹ J. Diefenbach,⁵ C. Djalali,¹⁰ B. Dongwi,⁵ L. El Fassi,¹ S. Gilad,⁷ K. Gnanvo,¹¹
R. Gothe,¹² K. Hafidi,⁴ D. Higinbotham,¹³ R. Holt,⁴ Y. Ilieva,¹² H. Jiang,¹² M. Kohl,⁵
G. Kumbartzki,¹ J. Lichtenstadt,¹⁴ A. Liyanage,⁵ N. Liyanage,¹¹ M. Meziane,¹⁵ Z.-E. Meziani,¹⁶
D. Middleton,¹⁷ P. Monaghan,⁵ K. E. Myers,¹ C. Perdrisat,¹⁸ E. Piassetzky,¹⁴ V. Punjabi,¹⁹
R. Ransome,¹ D. Reggiani,⁹ P. Reimer,⁴ A. Richter,²⁰ A. Sarty,²¹ E. Schulte,¹⁶ Y. Shamai,²²
N. Sparveris,¹⁶ S. Strauch,¹² V. Sulkosy,⁷ A.S. Tadepalli,¹ M. Taragin,²³ and L. Weinstein²⁴

¹*Rutgers University, New Brunswick, New Jersey, USA*

²*George Washington University, Washington, DC, USA*

³*Hebrew University of Jerusalem, Jerusalem, Israel*

⁴*Argonne National Lab, Argonne, IL, USA*

⁵*Hampton University, Hampton, Virginia, USA*

⁶*Duquesne University, Pittsburgh, PA, USA*

⁷*Massachusetts Institute of Technology, Cambridge, Massachusetts, USA*

⁸*Christopher Newport University, Newport News, Virginia, USA*

⁹*Paul Scherrer Institut, CH-5232 Villigen, Switzerland*

¹⁰*University of Iowa, Iowa City, Iowa, USA*

¹¹*University of Virginia, Charlottesville, Virginia, USA*

¹²*University of South Carolina, Columbia, South Carolina, USA*

¹³*Jefferson Lab, Newport News, Virginia, USA*

¹⁴*Tel Aviv University, Tel Aviv, Israel*

¹⁵*Duke University, Durham, North Carolina, USA*

¹⁶*Temple University, Philadelphia, Pennsylvania, USA*

¹⁷*Institut für Kernphysik, Johannes Gutenberg Universität, Mainz 55099, Germany*

¹⁸*College of William & Mary, Williamsburg, Virginia, USA*

¹⁹*Norfolk State University, Norfolk, Virginia, USA*

²⁰*Technical University of Darmstadt, Darmstadt, Germany*

²¹*St. Mary's University, Halifax, Nova Scotia, Canada*

²²*Soreq Nuclear Research Center, Israel*

²³*Weizmann Institute, Rehovot, Israel*

²⁴*Old Dominion University, Norfolk, Virginia, USA*

The Proton Radius Puzzle is the inconsistency between the proton radius determined from muonic hydrogen and the radius determined from atomic hydrogen level transitions and ep elastic scattering. No generally accepted resolution to the Puzzle has been found.

Here we propose a simultaneous measurement of μ^+p and e^+p scattering, as well as μ^-p and e^-p scattering, which will allow a determination of the consistency of the μp interaction with the ep interaction. The differences between $+$ and $-$ polarity scattering are sensitive to two-photon exchange effects, higher-order corrections to the scattering process. The slopes of the cross sections as $Q^2 \rightarrow 0$ are sensitive to the proton “radius”. We propose to measure relative cross sections at a typical level of a few tenths of a percent, which should allow the proton radius to be determined at the level of ≈ 0.01 fm, similar to previous ep measurements. The measurements will test several possible explanations of the proton radius puzzle, including some models of beyond standard model physics, some models of novel hadronic physics, and some issues in the radius extraction from scattering data.

^a This is an update of the MUSE proposal R12-01.1, originally submitted to the February 2012 PAC, for the January 2013 PAC.

CONTENTS

I. Beam Requirements	3
II. Physics Motivation	4
A. Introduction	4
B. Muon-Proton Scattering Experiments	5
C. Motivation Summary	7
III. Measurement Overview	7
IV. Experimental Details	10
A. Test Run	10
B. Beam	11
1. Requirements	11
2. Kinematics	11
3. Momentum Dispersion	12
4. Distinguishing Particle Types	13
5. Particle Fluxes	13
6. Beam Spot	15
7. Beam Systematics	15
C. Beam-Line Detectors	18
1. SciFi Detectors	18
2. GEM Detectors	19
3. Beam PID System	19
4. Beam Monitor Detectors	20
D. Target	20
E. Scattered-Particle Detectors	23
1. Overview	23
2. Spectrometer Detectors	25
F. Backgrounds	28
1. Pion and Muon Decays	28
2. Cosmic Rays	29
3. End Cap Scattering	29
4. Scattering from Upstream Detectors	30
G. Rates	30
H. Trigger	31
I. Radiative Corrections	32
J. Systematic Uncertainties	33
K. Cross Section and Radius Comparisons	34
V. Collaboration Responsibilities and Commitments Needed from PSI	35
VI. Safety Issues	36
VII. Technical Review Comments	37
VIII. Summary	41
References	41

I. BEAM REQUIREMENTS

- *Beam line:* π M1.
- *Beam properties:* Mixed $\pi/\mu/e$ beam. Fluxes of each particle type with 2.2 mA primary proton beam and full channel momentum acceptance are given in Table I. Channel acceptance will be limited to keep the total rate at the target to no more than about 5 MHz.

TABLE I. Beam flux at the target for full π M1 channel acceptance with 2.2 mA primary proton current. The total flux is based on previous measurements, while the relative fluxes of each particle types are based on MUSE test run measurements. Also shown in parentheses is the flux of each particle type when the combined flux is limited to 5 MHz.

Momentum (MeV/c)	Polarity	Total Flux (MHz)	π Flux (MHz)	μ Flux (MHz)	e Flux (MHz)
115	+	8.3	0.72 (0.43)	0.72 (0.43)	6.7 (4.04)
153	+	16.9	7.1 (2.10)	2.0 (0.59)	7.8 (2.31)
210	+	79.2	64.5 (4.07)	6.1 (0.39)	8.5 (0.54)
115	-	7.4	0.02 (0.01)	0.2 (0.14)	7.2 (4.86)
153	-	11.9	1.3 (0.55)	0.4 (0.17)	10.2 (4.29)
210	-	24.0	10.7 (2.23)	3.7 (0.77)	9.6 (2.00)

- *Duration of the experiment:* We expect the experiment to last at least three years. Tests measurements have been taken in late 2012, and we plan additional testing in May - June, 2013. The experiment requires 1 year of production running. With approval from PSI and funding made available in 2013, we can have equipment on site for a 1-month test run in early - mid 2015. Depending on any problems found and on beam schedules, a year long production run could start in late 2015 or early - mid 2016.
- *Special conditions:* none.
- *Beam time request for the first period after approval:* Additional beam tests in May - June, 2013.

II. PHYSICS MOTIVATION

A. Introduction

The *Proton Radius Puzzle* refers to the disagreement between the proton radius of 0.842 ± 0.001 fm determined by Pohl *et al.* [1] from muonic hydrogen and the values previously determined from atomic hydrogen transitions, 0.8768 ± 0.0069 fm in the 2006 CODATA analysis [2], and from *ep* elastic scattering, 0.895 ± 0.018 fm in the analysis of Sick [3].

In the 2.5 years since the Puzzle arose, it has been reinforced by the 2010 CODATA analysis [4] value of $r_p = 0.8775 \pm 0.0051$ fm. The CODATA analysis concluded that: “Although the uncertainty of the muonic hydrogen value is significantly smaller than the uncertainties of these other values, its negative impact on the internal consistency of the theoretically predicted and experimentally measured frequencies, as well as on the value of the Rydberg constant, was deemed so severe that the only recourse was to not include it in the final least-squares adjustment on which the 2010 recommended values are based.”

The Puzzle has also been reinforced by two recent *ep* scattering experiments. One of the electron scattering experiments was a precise cross section measurement [5] at Mainz that determined ≈ 1400 cross sections in the range $Q^2 = 0.0038 \rightarrow 1$ GeV². The Mainz analysis of only their data with a wide range of functional forms led to a proton electric radius of 0.879 ± 0.008 fm. The second experiment [6] at Jefferson Lab measured $\bar{e}p \rightarrow e'\bar{p}$ to determine 1% form factor ratios in the range $Q^2 = 0.3 \rightarrow 0.8$ GeV². An analysis of world data (excluding the Mainz data set but including the data analyzed in [3]) resulted in a radius of 0.870 ± 0.010 fm, consistent with the Mainz electric radius determination – although there were differences in the magnetic radius determination. A partial summary of recent proton radius extractions is shown in Fig. 1.

Thus, the Proton Radius Puzzle is arguably more puzzling now than when it first appeared. There has been wide spread interest in the Puzzle, and a number of articles published, with two review papers [7, 8] that we know of in preparation. The wide spread interest also led to a Proton Radius Puzzle Workshop [9] in Trento, Italy from Oct 29 - Nov 2, 2012. The workshop, organized by R. Pohl, G. A. Miller, and R. Gilman, included over 40 experts in various aspects of the Proton Radius Puzzle, discussing possible explanations and future experiments that might lead to data that would help to resolve the Puzzle. The meeting included atomic and nuclear theorists and experimentalists, as well as beyond-standard-model theorists. At the end of the workshop, a vote

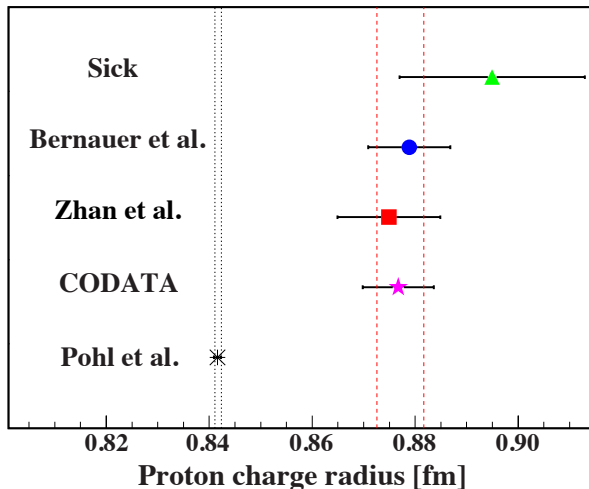


FIG. 1. A summary of some recent proton electric radius determinations; Sick [3], Bernauer *et al.* [5], Zhan *et al.* [6], CODATA [2], Pohl *et al.* [1]. Figure adapted from [6].

was held the likely resolution of the Puzzle. About one-third of the conferees were not willing to choose an option. The remaining two-thirds of the conferees were about equally split between two alternatives:

- *Beyond standard model (BSM) physics.* Several models that cannot be ruled out have been introduced of BSM physics that could lead to the radius extraction from muonic hydrogen being incorrect. Typically they involve pairs of new particles which have limited ranges of coupling constants, and are somewhat nonnatural, as, for example, there would be a force between first-generation quarks and second-generation leptons not present between first-generation quarks and first-generation leptons. Of particular interest here is the work of Batell, McKeen, and Pospelov [10] as it predicts enhanced parity violation in muon scattering, which might be possible to measure in a second-generation experiment following this proposal.
- *Issues in the ep data.* There is a significant possibility that the precision of the atomic hydrogen experiments is overstated in the CODATA analyses, as many of the experiments have been done by the same group and the results are not entirely independent. For the ep scattering, while most of the ep analyses get a radius of about 0.875 ± 0.01 fm, there are two analyses that obtain radii 0.84 - 0.85 fm. These two analyses were both sharply criticized at the workshop, but they suggest that the uncertainties in any of the individual radius extractions are probably optimistic.

There have been a number of suggestions as to how the puzzle could possibly be resolved by hadronic physics / proton structure considerations, but there was little support for any of these ideas among the conferees. A subset of these ideas have the general feature that they predict enhanced two-photon exchange effects, at the level of a few percent, which could be detected in this experiment.

A number of experiments that might help resolve the Puzzle were discussed at the Workshop. Efforts to perform new atomic hydrogen experiments in the next 5 - 10 years could help confirm the Puzzle exists, or instead indicate consistency in the muonic and electronic atomic physics measurements. A new muonic deuterium experiment can be compared with the electron-deuteron radius measurements to check for consistency. A new Jefferson Lab experiment [11] approved by PAC39 plans to measure very low Q^2 electron scattering, from $\approx 10^{-4}$ GeV² to 10^{-2} GeV², perhaps as early as 2015. We quote from Jefferson Lab PAC38: “*Testing of this result is among the most timely and important measurements in physics.*” The efforts of the MUSE collaboration – this proposal – to compare $\mu^\pm p$ and $e^\pm p$ elastic scattering were also discussed. The Workshop conferees strongly supported all of the experimental efforts; since the origin of the Puzzle is uncertain, it is not clear which possible experiment will give us the data that resolves the Puzzle.

B. Muon-Proton Scattering Experiments

The differences between the proton radius measured in the μp system and in ep systems is a surprise in part due to lepton universality being generally accepted. Tests of the equivalence of μp and ep systems from a few decades ago provided direct constraints on violations of and possible differences between ep and μp interactions. We give two examples here.

The radius of ¹²C is one of the most precisely determined radii from electron scattering. The electron scattering result [12] is $\langle r^2 \rangle^{1/2} = 2.472 \pm 0.015$ fm, based on scattering of 25 – 115 MeV electrons at momentum transfers from 0.1 – 1.0 fm⁻¹, or $Q^2 \approx 0.0004 - 0.04$ GeV². A subsequent analysis of world data [13] found that dispersive corrections increase the extracted radius to 2.478 ± 0.009 fm. The charge radius was also measured by determining the ≈ 90 keV X-ray energies in muonic carbon atoms to several eV [14]. Assuming a harmonic oscillator nuclear charge distribution led to a ¹²C radius of $\langle r^2 \rangle^{1/2} = 2.4715 \pm 0.016$ fm. A subsequent muonic atom experiment [15] found $\langle r^2 \rangle^{1/2} = 2.483 \pm 0.002$ fm. There is evidently no μp vs. ep issue in the carbon radius determination. There are several possible reasons why there might be a μ / e difference in the proton but not in carbon. Examples include opposite effects in the case of μn vs. μp interactions,

and the charge distribution in carbon resulting largely from orbital motion of the nucleons, in which there is no effect, vs. charge distributions of the nucleons, in which there is an effect.

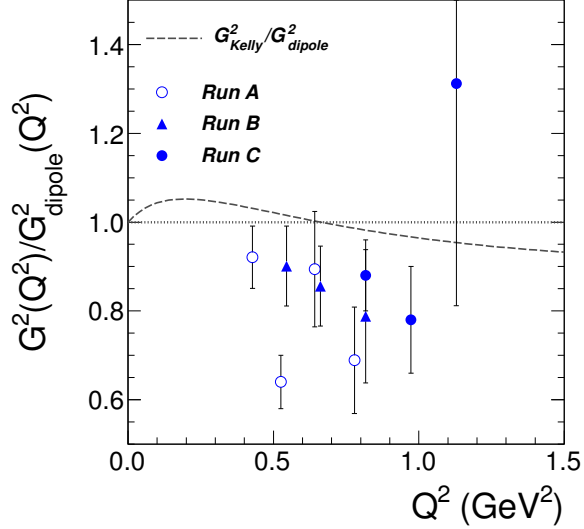


FIG. 2. Reduced cross sections, $d\sigma/d\Omega/d\sigma/d\Omega_{Mott}$, for μp elastic scattering, from Ellsworth *et al.* [16]. The data are somewhat below expectations from the dipole form factor parameterization. Use of the more modern Kelly parameterization [17] does not qualitatively change the result.

One of the better early μp elastic scattering experiments was Ellsworth *et al.* [16], which found that cross sections in the range $Q^2 \approx 0.5 - 1 \text{ GeV}^2$ were about 15% below the standard dipole parameterization, $G_E = G_M/\mu_p = (1 + Q^2/0.71)^{-2}$ with Q^2 in GeV^2 , and a similar percentage below modern form factor fits. as shown in Fig. 2. While this suggests an ep vs. μp interaction difference, Ellsworth *et al.* interpreted the difference as an upper limit on any difference in μp and ep interactions. These data are too high in Q^2 to make any inferences about the proton radius. A subsequent experiment [18] covering $0.15 < Q^2 < 0.85 \text{ GeV}^2$ found μp cross sections about 8% smaller than the electron scattering results, similar to [16], and considered the μp and ep scattering results consistent within uncertainties. A final elastic scattering experiment [19] analyzed the ratio of proton elastic form factors determined in μp and ep scattering as $G_{\mu p}^2/G_{ep}^2 = N(1 + Q^2/\Lambda^2)^{-2}$, with the result that the normalizations are consistent with unity at the level of 10%, and the combined world μp data give $1/\Lambda^2 = 0.051 \pm 0.024 \text{ GeV}^{-2}$, about 2.1σ from the electron-muon universality expectation of 0. For deep-inelastic scattering [20], a similar analysis yields a normalization consistent with unity at the level of 4% and $1/\Lambda^2 = 0.006 \pm 0.016 \text{ GeV}^{-2}$. In summary, old comparisons of ep and μp elastic scattering have sometimes indicated several percent differences between μp and ep with similar size uncertainties, or sometimes indicated consistency with several percent uncertainties. The directly measured constraints on differing μp and ep interactions are not very good. While ep studies have advanced significantly in the past decade, the μp work has not.

Two-photon exchange effects have also been tested in μp scattering. In [21], no evidence was found for 2γ effects, with μ^+p vs. μ^-p elastic scattering cross section asymmetries consistent with 0, with uncertainties from $4 \rightarrow 30\%$, and with no visible nonlinearities in Rosenbluth separations at $Q^2 \approx 0.3 \text{ GeV}^2$. The Rosenbluth cross sections were determined to about 4%. Tests in ep scattering [22] have found no nonlinearities even with $\approx 1\%$ cross sections; improved experiments are underway [23]. Current best estimates of the size of the nonlinearities in Rosenbluth separations

for ep scattering are at the percent level.

To summarize, direct comparisons of μp and ep scattering were done, but only with overall precisions at the $\approx 10\%$ level. The comparisons were also at sufficiently large Q^2 that they would not be sensitive to the proton radius. Measurements sensitive to 2γ exchange were also performed, but at a level that we now believe is not sufficiently precise to provide significant results.

C. Motivation Summary

The Proton Radius Puzzle has attracted wide interest, but the resolution to the Puzzle is unclear. It might arise from beyond standard model physics, novel hadronic physics / proton structure, or issues and / or underestimated uncertainties in the determination of the radius from the actual experimental data. There is strong support in the community for a number of experiments that test different explanations for the Puzzle. New ep atomic physics and scattering experiments are planned, as are additional muonic atom experiments. The MUSE proposal presented here is the only proposed direct test of ep vs. μp , in a scattering experiment. It also directly measures 2γ exchange effects.

III. MEASUREMENT OVERVIEW

First, we note that this is an update of proposal R12-01.1 submitted to PSI in February 2012. The collaboration subsequently underwent a technical review in July 2012. The comments of the technical review committee and responses to them are reproduced in Sec. VII. The collaboration subsequently performed test measurements with the $\pi M1$ beam line; a report is available [24].

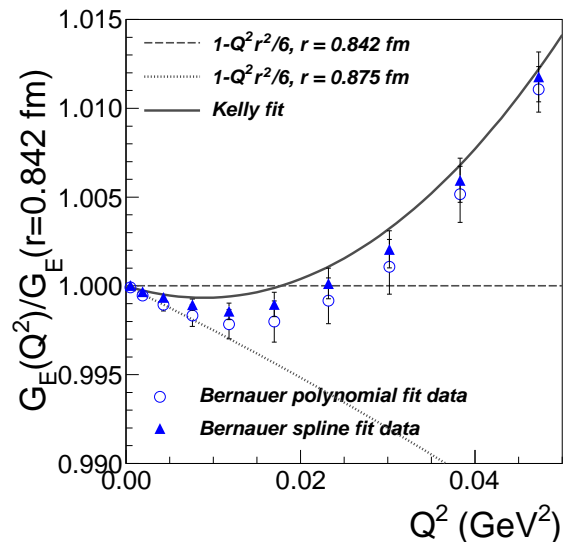


FIG. 3. Mainz results [5] for the proton electric form factor determined by spline and polynomial fit analyses of the cross sections, along with the Kelly parameterization and a linear fit assuming the radius determined by ep measurements, all relative to expectations from a linear fit using the radius determined from μp atoms. The data show that there is curvature in the form factors indicative of higher order contributions beyond the radius term. The very lowest Q^2 data are more consistent with a larger radius.

Our approach to resolving the Proton Radius Puzzle is to measure simultaneously elastic $\mu^\pm p$ scattering and $e^\pm p$ scattering. We will make comparisons to ep scattering at the cross section level, with extracted form factors, and ultimately with an extracted radius. The basic idea is that, if the μp and ep interactions are different, this should be reflected in the scattering experiment as well as in the atomic vs muonic hydrogen measurement. Thus the experiment most directly tests the most interesting possible explanations of the proton radius puzzle, that there are differences in the μp and ep interactions.

An indication of how well the experiment needs to be done is shown in Fig. 3. First, it is clear that curvature starts to become apparent in the form factor by $Q^2 \approx 0.02 \text{ GeV}^2$, so the experiment needs to measure a significant fraction of the Q^2 range below 0.02 GeV^2 , as well as measuring the region above to constrain higher order terms in the form factor expansion. Second, the form factor only varies by a few tenths of a percent between what one expects if $r_p = 0.84$ vs. 0.88 fm , so precise cross sections are needed. If the form factor varied linearly with Q^2 , the cross section would change by about 0.5% (1%) at 0.01 (0.02) GeV^2 from the change in radius. In the case of the Mainz experiment, the absolute cross sections were not measured very precisely, but the relative cross sections were, allowing the data to be normalized with a single normalization factor for a number of data points along with a fit that goes through the $Q^2 = 0$ point: $G_E^p(Q^2 = 0) = 1$. We will not be able to achieve sub-1% level absolute uncertainties, so we will also be forced to normalize the data with a fit, to determine the absolute normalization. Thus, it is really the point-to-point systematic uncertainties that are crucial for the experiment to succeed.

An important point we can learn from the Mainz experiment that is not so evident from this very brief discussion is that the overlap of multiple kinematic settings is an important test of the quality of the experimental data. In the Mainz experiment data were taken at 6 different beam energies with multiple spectrometers with overlapping angle ranges, and subdivided into 31 sets for fitting. While we do not have as great a beam energy range and thus kinematic flexibility as the Mainz measurement, we plan to take data with both positive and negative beam polarities at 3 different energies with two large acceptance spectrometers. Statistical precision is at the 1% level for our largest angle, lowest rate measurements, and significantly better for forward angles. Point-to-point systematic uncertainties are estimated to be at the few tenths of a percent level. There are a number of overlaps that will allow the estimated experimental systematics to be studied, including:

- Each angle range can be subdivided into multiple azimuthal angle ranges during the analysis phase, and the comparison can be used to test the systematics.
- We initially plan for one high statistics comparison measurement with the spectrometers offset by a small angle as a cross check. This should be sufficient, though we leave open the possibility of requesting additional such cross checks based on the actual data.
- The use of multiple energies with significant overlap in Q^2 allows numerous overlaps of the same form factors measured at different energies and angles.

Beyond proposing simply measuring μp scattering, it is important that we measure scattering of both polarities of μ 's and e 's. These data directly test whether 2γ exchange could be significant, altering the radius extracted in the scattering experiments from its true value, and also test certain hadronic physics ideas that lead to enhanced 2γ exchange. The correction is believed, based on model calculations and data, to be small for low Q^2 ep scattering. Calculations typically estimate the corrections to be at the percent level – only at the few tenths of a percent level for the kinematics of this proposal – while constraints from e^+p to e^-p comparisons are typically limits at the level of a few percent. An interesting feature of this experiment is that the 2γ exchange effect depends not only on Q^2 but also on the scattering angle. The 2γ exchange corrections in theoretical models generally decrease for constant Q^2 as the energy of the beam increases and the scattering angle decreases. Since this experiment runs at lower energy than the experiments running at electron machines, the scattering angle is larger and the 2γ exchange effect might be as well. Thus, this proposal will be unique in having not only μ^\pm but also e^\pm comparisons at large angles and low Q^2 , exactly the region of interest.

The comparison of normalized cross sections and form factors and their Q^2 variation will be the highest precision comparison we can make for differences in μ 's and e 's, or for two-photon effects. When data are fit, the values of the cross sections and form factors will be known at the level of a few tenths of a percent in the range of the data, as was the case with the Mainz measurement. However, the uncertainty on the radius will be at about the percent level, a few times worse, and thus will not constitute as precise a test of μ vs. e flavor independence. Our intent is also to make a comparison of our ep data with the Mainz ep data, as a check on our ep extraction.

The discussion so far has focused on the elastic scattering reactions as if backgrounds did not exist, but there are several backgrounds, most of which can be cut from the analysis, but some of which need to be subtracted from the analysis. Important examples include:

- The most obvious background, π induced reactions, has rates as high as 150 kHz, which would swamp the data acquisition system. Readout of these reactions is suppressed by a factor of about 10^5 at the trigger level, limited due to misidentification of π 's as e 's or μ 's by the beam PID system, and suppressed to a negligible level at the analysis level.
- Accidental coincidences of π 's scattering events with beam e 's and μ 's occurs at levels up to about 3 kHz. Inefficiencies in detecting π 's with the beam PID system at the 2% level will allow about 60 Hz of these events through. They can be eliminated at the analysis level.
- Decays of μ 's in flight lead to up to a few hundred Hz of triggers, which cannot be avoided. At the analysis level, cuts on target position and time reduce these events by about 90%, leading to about an order of magnitude more events than for elastic scattering. This rate has to be measured and subtracted, and will increase the uncertainties about a factor of 3.
- Scattering from target end caps cannot be removed at the trigger or analysis levels. It is removed by cuts, though these are not effective at the most forward angles due to decreased z -target resolution, and by measurement and subtraction.

For the following discussion, it should be noted that we envision the experiment running in three stages. The first stage is the period in which we are seeking funding for the experiment and constructing the experimental equipment. Throughout this period we expect to have a series of test measurements. The first such measurements, to check beam properties and simulations, were done in fall 2012, with fast scintillators and scintillating fibers. Additional measurements, to further test beam properties and simulations and some detector options, are planned for May/June 2013. For these measurements we expect to have the OLYMPUS GEMs available, which will allow us to more precisely determine beam properties.

The second stage of the experiment will use the new equipment for a two-month long “dress rehearsal” of the experiment. Carrying this out first requires a ≈ 6 month period for installation and commissioning of detectors, including various systematics studies which are in part described in this proposal. The goal is to essentially take one of the planned data points, analyze it, and confirm that the performance of the experimental detectors and the rejection of backgrounds is satisfactory with the actual hardware setup. We expect that, with PAC approval and funding available in 2013, we could be ready for the second stage of the experiment to start in late 2014 or early 2015. This will require a several month analysis period.

Once we confirm the performance of the experiment is satisfactory, the third stage of the experiment will be the production run, measuring elastic scattering cross sections with both beam polarities at three beam momenta, $p_{in} \approx 115$ MeV/ c , 153 MeV/ c , and 210 MeV/ c . We expect the third stage of the experiment to start in mid or late 2015 and plan on 12 months of beam time.

To summarize, we expect:

- to simultaneously determine $\mu^\pm p$ and $e^\pm p$ elastic scattering cross sections,
- to compare the ep cross sections with world data,
- to compare the $\mu^\pm p$ and $e^\pm p$ cross section to test 2γ exchange,
- to compare the μp and ep cross sections and form factors for a direct test of lepton universality,

- to extract proton radii from the measurements for a check of consistency within the experiment, and with the world data.

The experiment will study multiple physics issues: basic and novel 2γ exchange effects, lepton flavor universality, proton form factors, and the proton radius. Based on the Mainz cross sections, successfully carrying out the experiment requires that cross sections be determined at the tenths of a percent level (relative) over the low Q^2 region, from below 0.01 GeV² to at least 0.04 or 0.05 GeV². Our planned kinematic range covers about 0.002 to 0.07 GeV².

IV. EXPERIMENTAL DETAILS

A. Test Run

This is an update of the MUSE proposal R12-01.1, originally submitted to the February 2012 PAC, for the January 2013 PAC. The collaboration generated a Technical Design Report in June 2012 [25] which was reviewed in July 2012. Several concerns were expressed by members of the PAC and the technical review committee about whether the π M1 beam properties were sufficient to run the proposed MUSE experiment. During fall 2012, nine members of the MUSE collaboration came to PSI for periods ranging from a few days to 3 months to perform test measurements, along with PSI based collaborators. A separate report [24] on the test measurements is available. Following is the summary of the results, taken from the report summary.

During fall 2012, the MUSE collaboration undertook a series of beam studies in the PSI π M1 channel to check whether the channel is suitable for measuring precise μp and ep elastic scattering cross sections. Many of the potential issues suggested to us turn out to not be issues, but some issues arose which lead to modest changes in our plans. The positive results reported here include the following:

- *One concern expressed was that the time-width of the proton beam is about 1 ns, which would prevent our identifying particle types in hardware.* We find that the time-width is 250 - 500 ps (σ), and is not an issue, given the ≈ 1.25 ns binning planned for hardware particle identification.
- *One concern was that the sizes of the π , μ , and e beams at the target are different.* We found no significant difference between the π , μ , and e distributions in our SciFi array at the target position. There is a small indication that the π beam is slightly wider, perhaps due to μ 's from π decays near the target being identified as π 's. This finding needs further study once the beam tune is further developed.
- *One concern was that the momentum dispersion of π 's, μ 's and e 's would be different at the intermediate focal point.* We studied the time variation of π , μ , and e RF time peaks as a narrow collimator about 0.14% wide in momentum was moved between nominal positions of -0.8%, 0%, and 0.8% in δ . The shifts in the peaks was consistent with a 0.6% shift, basically consistent with the expected dispersion given the uncertainties in the beam tune and measurements. This finding needs further study once the beam tune is further developed.
- *One concern was that the distribution of different particle types is different at the IFP.* We find that essentially all particles that reach the target are within the envelope calculated for pions with TURTLE, a region at the IFP that is about 5 cm high by 20 cm wide.
- *One concern was with high proton rates in positive polarity.* We find no significant proton rate for the momenta of this experiment.

A more extensive discussion of the test run can be found in the test run report [24].

As with any measurement, carrying out the test run involved encountering and resolving a number of problems dealing with magnets, detectors, electronics, and data acquisition, which do

not affect the results reported above. One problem that continues to be worked on is improving the tune of the π M1 channel. The data were largely taken with a beam spot a few cm wide in the nondispersive direction by several cm wide in the dispersive direction. After the main measurement period a better tune was developed that focused the beam to a few cm wide spot on target in each direction. With the new tune we reconfirmed that there is no significant difference between the distributions on target of the different particle types.

This new tune still provides a beam spot a few times larger than the about 1 cm by 1.5 cm beam spot used many years ago. We do not believe that the issue of the channel tune is a fundamental problem. It should not be surprising, when the channel has not been used to generate a small beam spot in many years, that redeveloping the tune takes more than a few days of work.

B. Beam

1. Requirements

The experiment requires that we obtain from the π M1 beam line the following:

- a momentum range of about 100 - 200 MeV/ c , to obtain a range of kinematics,
- momentum dispersion of the particles at the IFP, to know the incoming particle momentum better than the channel full acceptance,
- distinguishable π 's, μ 's, and e 's, to be able to count the beam particles for normalization and to trigger only events of interest,
- a good fraction of MHz fluxes of e 's and μ 's at minimum, so that the experiment can be run in a reasonable time, and
- a well focussed beam spot, to reduce backgrounds and minimize cryotarget size.

Many but not all of these features were confirmed in the test run briefly described above. In this section we review these basic requirements and the beam line detectors that will be used.

2. Kinematics

Figure 4 gives an overview of the range of kinematics accessible with the π M1 beams. Measurements outside the range 100 - 250 MeV/ c are difficult or less interesting for a number of reasons. The Mainz [5] Q^2 range was $\approx 0.0038 - 1$ GeV². From the varying analyses of the data sets, given that the data are normalized as part of the fitting using a fit constraint at $Q^2 = 0$, we conclude that it is important to go to as small a Q^2 as possible to constrain any determination of the radius; adjusting normalization of data sub-sets is required as the systematic uncertainties on the absolute cross sections will not be sufficient to allow a precise radius to be extracted. As will be discussed further below, our planned beam momenta are about 115, 153, and 210 MeV/ c , which allow access to $Q_{min}^2 \approx 0.0015, 0.0025, \text{ and } 0.005$ GeV², respectively. Each beam momentum roughly cuts in half the minimum Q^2 of the next higher beam momentum, allowing a better radius determination. While the Mainz kinematic range is much larger than ours, the important coverage for determining the radius is the region below about 0.02 GeV², where nonlinear behavior in the form factor starts to become apparent, along with enough coverage at higher Q^2 to constrain higher order terms. Thus, we can obtain a similar quality radius extraction as in [5] if we can maintain good systematic and statistical uncertainties over our smaller, but lower, kinematic range.

Figure 4 also gives an estimate of the magnetic contribution to the cross section, based on the Kelly form factor parameterization [17]. In the Q^2 range of this experiment, the variations in the extracted magnetic form factor from various recent fits are at the level of $\pm 1\%$, despite the 10% difference in the extracted magnetic radius from recent fits. Thus, as long as the magnetic

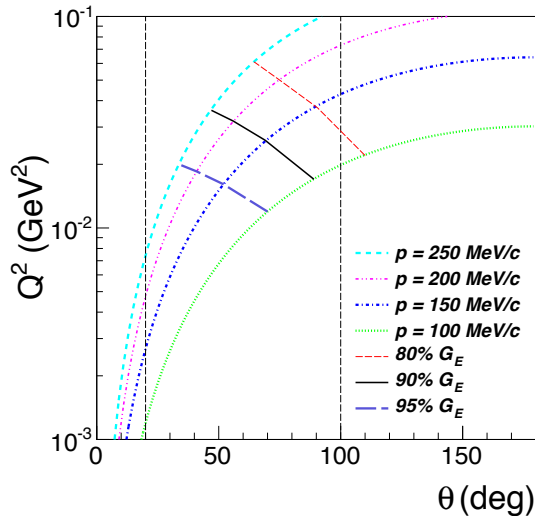


FIG. 4. Q^2 vs. θ for different incident beam momenta. Also shown are lines that indicate where the electric response leads to 80%, 90%, and 95% of the total cross section. The vertical lines at $\theta = 20^\circ$ and 100° indicate the planned angular range of the measurements.

contribution to the cross section is about 10% or less, the uncertainty in the extracted electric form factor from the measurement will be at the level of 0.1%, which is within our desired uncertainty budget. There are several ways in practice of handling the magnetic contribution, including using existing electron scattering results, and doing an independent fit to our data of G_E and G_M . The uncertainty due to G_M doesn't impact the *comparison* of ep to μp , or of μ^+p to $|mu^-p$, although it could have an impact on the extractions of r_p if a difference is observed in the electron and muon cross sections. If there are either significant 2γ exchange effects or significant differences between μ 's and e 's, these are significant findings by themselves even if they impact determinations of r_p by preventing our use of existing G_M data.

3. Momentum Dispersion

As discussed before, initial measurements taken during the test beam period with a non-optimal beam tune showed through RF time variations of the π 's and μ 's that there was a momentum dispersion of the particles at the IFP about of the magnitude expected.

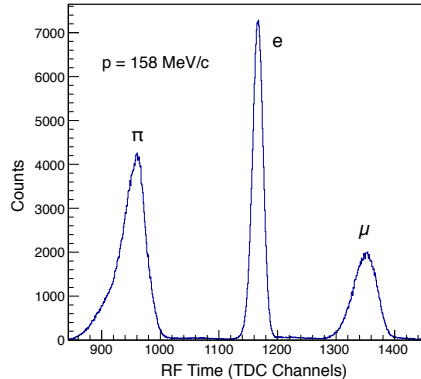


FIG. 5. Counts vs. RF Time spectrum from the MUSE testrun. The horizontal axis is TDC channels, with each channel equal to 25 ps. The data were taken with a 0.1 mA primary proton beam current and a π M1 channel momentum of 158 MeV/c with positive polarity. The spectrum was measured with fast scintillators about 23 m from the M1 production target, which were read out through a CAEN v1290 TDC. From left, the three peaks are π 's, e 's, and μ 's.

4. Distinguishing Particle Types

We identify the particle types through RF time measurements, the time of the particles in detectors relative to the accelerator RF. Since the accelerator operates at ≈ 50 MHz, the RF time represents when the proton beam pulses go through the M1 production target, with some offset and modulo 20 ns. The time between a particle reaching a scintillator and the RF time signal then represents the time of flight of the particle through the π M1 channel, with some offset and modulo 20 ns. A sample RF time spectrum from the test run is shown in Figure 5; the π , e , and μ peaks are clearly distinguishable.

There are 3 momenta at which the particles can be well separated with RF time measurements at the target. The exact momenta which optimize the separation depend on the target detector position, and will be chosen for the run based on the as-built detector configuration. Here we work with our nominal beam momenta choices of 115, 153, and 210 MeV/c. We plan to suppress backgrounds by measuring the RF times of particles at two positions, at the IFP where the beam is momentum dispersed, about 12.2 m from the M1 production target, and just upstream of our scattering target, about 23 m from the M1 production target. Figure 6 shows simulated spectra. (Note that because the test run TDCs were in common stop mode, the order of the peaks in Figure 5 is opposite the order in Figure 6.) One can see that the peaks are generally well separated even though the momenta are not optimized. The measurement of the RF time at the IFP will further suppress background triggers.

Particularly at 115 MeV/c it is possible to see that the time of flight of the particles from the IFP to the target provides an additional means of PID in hardware. The $e / \mu / \pi$ flight times are shown in Table II. By fine tuning the timing of the RF time signal relative to the trigger signal, it should be possible to make the π 's correspond to one more RF bucket between the IFP and target times than for the e 's or μ 's. Thus, when forming a coincidence of μ RF times, for example, a single π would never generate a coincidence since it is 20 ns out of time.

5. Particle Fluxes

The π M1 channel e^\pm and π^\pm fluxes were measured long ago, but μ^\pm fluxes were not so well known. During the test run, we measured the relative numbers of π 's, μ 's, and e 's for both polarities. Using previous e and π flux data for absolute normalizations, we calculated the absolute

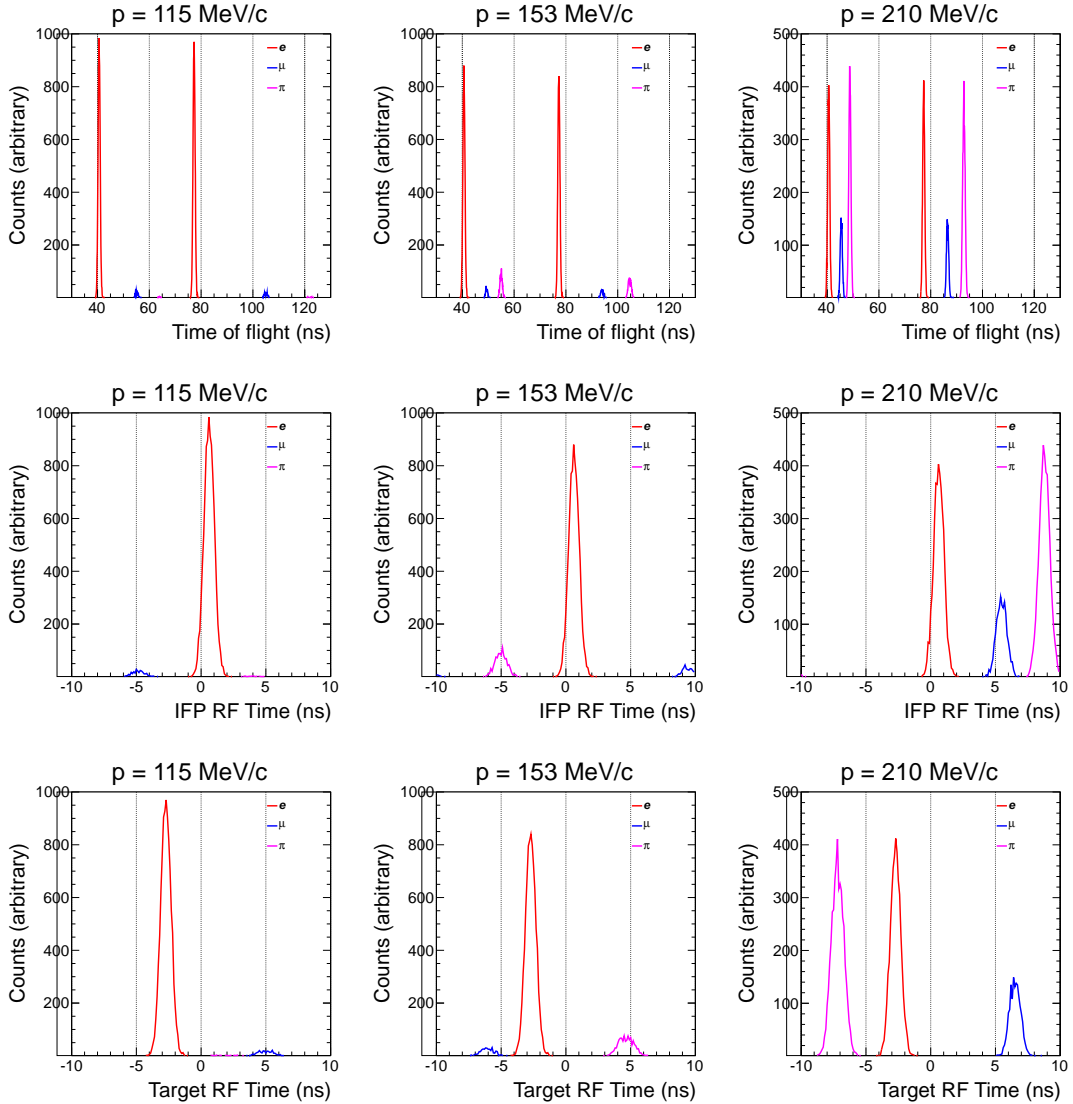


FIG. 6. Simulated time and RF time spectra for three different beam momenta. The top row shows the actual flight time of the particles to both IFP (times around 40 - 60 ns) and target (times around 75 - 120 ns) detectors. The middle row shows the RF time at the IFP. The bottom row shows the RF time at the target. For this simulation the IFP and target detectors were 12.2 and 23.2 m flight paths from the M1 target. The electron peak is 0.4 ns (σ) wide; the μ and π peaks are 0.4 ns wide folded with the variation in time due to the β variation from the 3% channel momentum bite. These widths are consistent with those seen during the test run, with high resolution scintillators and TDCs. The relative numbers of particles are based on our negative polarity measurements during the testrun.

fluxes given in Table I, for 2.2 mA of primary proton beam current.

The flux at which we can run is limited. We need to be able to cleanly identify e 's and μ 's, and we need to avoid accidental coincidences with π 's, as π scattering events are much more likely than μ or e scattering events. Also we need to limit random backgrounds in the detectors. The target SciFi detector has a limited number of channels, because the beam spot near the target is small, which caused us earlier to suggest limiting the beam flux to 10 MHz on target. We now see from test runs that rates at the IFP are significantly higher. Some of the higher rate arises from π 's

TABLE II. Flight times and flight-time differences between IFP and target detectors. The β variations within the channel acceptance lead to time variations of up to 0.5 ns.

Momentum (MeV/c)	TOF _e (ns)	Δ TOF _{$\mu-e$} (ns)	Δ TOF _{$\pi-e$} (ns)
115	36.7	13.0	21.0
153	36.7	7.8	13.0
210	36.7	4.3	7.4

that decay before reaching the target, some arises from particles within the channel acceptance up to the IFP but not up to the target, and some arises from the neutron flux through the channel to the IFP region. A neutron rate in the test run detector of about 30 MHz was measured; the more properly sized detector we intend to construct for the experiment will have a smaller neutron flux of no more than about 5 MHz. For now we plan to be more conservative and limit the rate at the target to only 5 MHz. This will lead to μ fluxes in the range 0.14 - 0.77 MHz, as shown in Table I and electron fluxes of 0.54 - 4.86 MHz.

An important point already seen in the test run and in previous measurements is that when π 's decay to μ 's (and ν 's) near the target detector, the time measured in the target SciFi detector is still that of a π , so any scattering event from this particle will not lead to a trigger. The particle will be considered by the beam PID system to be a π .

6. Beam Spot

During the test run, the π M1 tune had not been well reestablished, and the measurements were taken with a broad beam spot, particularly in the x direction. Subsequently, an additional few days of work by the PSI group reduced the beam spot size to 25 mm (σ_x) by 14 mm (σ_y) at 153 MeV/c, with a slightly smaller spot at higher momentum and a slightly larger spot at lower momentum. While much improved, this result still does not match the nominal channel spot size. At the time of this writing, additional work on the beam tune is planned for December 2012.

Using a target SciFi array during the test run, we studied the target distributions for different particle types, for the poor and improved tunes mentioned above. We found no significant difference between the distributions of the different particle types at the target. There was a slight indication that the pion distribution is slightly larger than the muon or electron distributions, which we speculate is due to tails from pion decays to muons just before our detector array – these are still read out as our trigger scintillators are 50 cm wide.

7. Beam Systematics

An important issue is the sensitivity of the measurement to the beam properties. Here we discuss the sensitivity to the beam momentum and flux, and to the knowledge of the scattering angle. We emphasize in advance that the comparisons of, for example, e to μ or of μ^+ to μ^- are insensitive to many of the systematics, as the systematic leads to either a similar shift to both data sets, so the comparison is largely unaffected, or the systematic shifts act largely like a renormalization, and we expect in fitting to adjust the data set normalizations.

Figure 7 shows the sensitivity of the cross section measurement to offsets in the beam momentum. The correction is different for μ 's and e 's due largely to mass-dependent terms in the complete cross section formula. Since the cross section depends on the form factors squared, effects on the form factors are half as large as on the cross section – the $\approx 0.05\%$ point-to-point variations become 0.025% in the form factors, and the 0.1 - 0.2% overall changes become 0.05 - 0.1% absolute uncertainties in the form factors. This uncertainty is tolerable. Thus, knowing the beam momentum to 0.1% is sufficient.

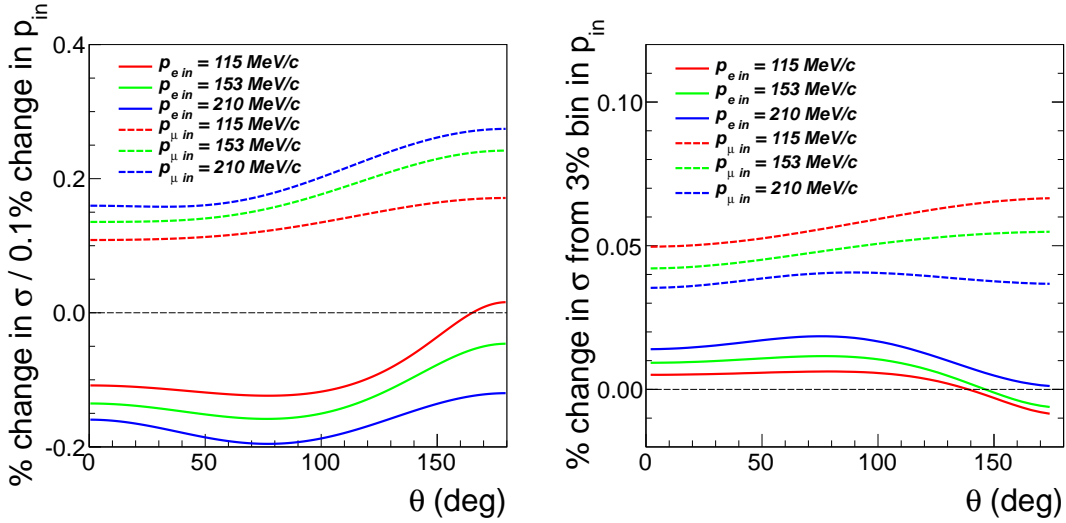


FIG. 7. Left: sensitivity of the cross section to changes in the beam momentum. Right: effect of averaging the cross section over a $\pm 1\%$ momentum bin. Estimates were made using the Kelly form factor parameterization.

The beam momentum can be determined from the RF times of the π vs μ vs e peaks. A 0.1% momentum change shifts the π and μ peaks by about 28 and 17 ps respectively at 210 MeV/c (72 and 48 ps at 115 MeV/c). As the high precision scintillators we will use have better than 50 ps resolution, but the RF time peaks in the test run were about 500 ps (σ) wide, one can see that the beam momentum can be determined to about 0.1%.

One thing to consider is whether the difference in the systematic offsets between μ 's and e 's can be used to help determine a beam momentum offset when fitting a common form factor parameterization to both μp and ep scattering data. For testing if the data can be consistent with the same form factors for e 's and μ 's this can be tried, but one must remain aware of the possibility that there is a difference between μ 's and e 's that happens to make a more or less overall shift between the two that resembles a beam momentum offset.

Figure 7 also shows that the determination of the cross section is very insensitive to averaging over a $\pm 1.5\%$ momentum acceptance of the π M1 channel, but this result is based on the flux being independent of momentum. While the electron flux does not vary very strongly with momentum in our kinematics, the muon flux appears to be decreasing quickly at our lowest momentum. Since changing the momentum does change the cross section, as also shown in Figure 7, it appears that the most sensible way to limit the beam flux is to collimate at the IFP to limit the 3% momentum acceptance of the π M1 channel.

Figure 8 shows a GEANT simulation of the muon beam momentum distribution at the target. Note that the vertical scale is logarithmic. The relative shifts in the spectra are somewhat smaller at 210 MeV/c, but somewhat larger at 115 MeV/c. One sees that for the muons that the spectrum coming from the channel is shifted by about 3% in the middle of the target, and about 1% broader. We can conclude from this that the simple averages done above to show the sensitivity to the beam offsets and averaging are appropriate for the muon cross sections. However, it will be important for the experiment to validate the simulations. Our basic technique to do this is to have dedicated test measurements in which we measure the spectrum without and with detectors in the IFP region, to check for momentum shifts, and measure multiple scattering from detector and target elements by putting GEM telescopes both before and after them.

It is obviously necessary to determine the beam flux precisely to measure a precise cross section. Our plan to do this is to use beam line detectors to count the number of beam particles of each

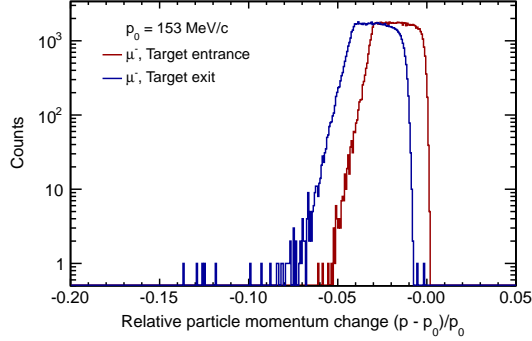


FIG. 8. GEANT simulation of the muon beam momentum spectrum incident upon and exiting the liquid Hydrogen target at a beam momentum of 153 MeV/c. The beam initially had a uniform distribution with a 3% momentum bite, but was broadened mainly due to interactions with the target SciFi and GEM detectors.

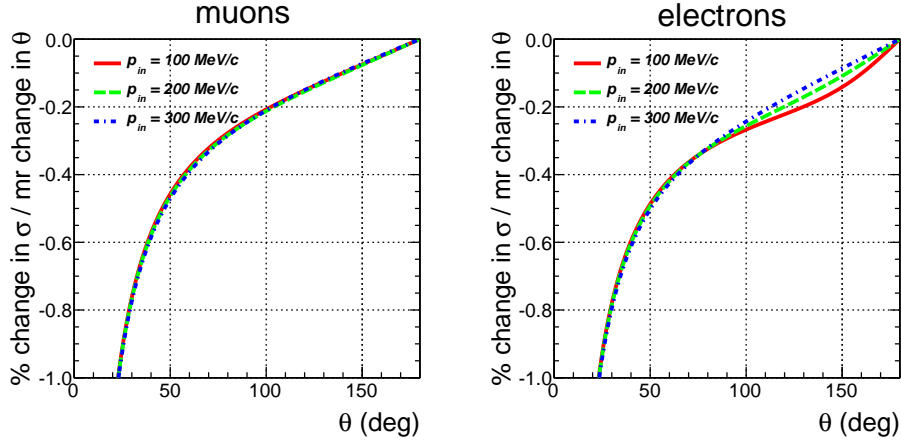


FIG. 9. Sensitivity of the cross section to changes in the scattering angle. The increasing systematic uncertainty at small angles can be understood from the $\approx 1/\sin^4(\theta/2)$ dependence of the Mott cross section; this strong variation at small angles from angle offsets is one of several reasons cross section measurements will be limited to about $20^\circ < \theta < 100^\circ$.

type. Since our trigger will require a particle in the beam that is identified as either an e or a μ , a counting inefficiency for e 's or μ 's does not affect the cross section, but misidentifying a particle of another time or perhaps random coincidence backgrounds as an e or a μ is an issue.

Since the number of beam particles counted is the same for all angles measured at the same time, the relative error for the beam flux is small. There is a single overall normalization factor for each setting that we expect to determine from fits of the six different experimental settings – three momenta times two polarities. Still, our intent is to precisely determine the beam flux in particular since beam momentum offsets act largely like normalization errors.

The π M1 web pages [26] give a spot size on target of 1.5 cm horizontal by 1 cm vertical, with angular divergence of 35 mr horizontal by 75 mr vertical.¹ (Alternate beam tunes are possible, and some older experiments achieved beam spots smaller than 1 cm (σ) in each direction.) But offsets

¹ Note that no measurements were done of the beam divergence during the test run. We expect the OLYMPUS GEMs to be available in 2013, allowing these measurements to be done during a May/June test run.

in the scattering angle at the mr level lead to significant changes in the cross section, as shown in Fig. 9. Thus the orientation of the detectors relative to the beam should be known at the sub mr level. Because this is so much less than the angular divergence of the beam, 35 mr horizontal by 75 mr vertical, it is clear that this cannot be achieved unless we determine incoming trajectories on an event by event basis much more precisely with beam chambers. This leads to our decision to use GEM chambers in the beam line. The angle for each event should be known at the several mr level, but the angle knowledge will be limited by multiple scattering rather than by the chambers.

C. Beam-Line Detectors

The beam line detectors have to operate at high rates, which we now plan to limit to 5 MHz at the target, and a few times higher at the IFP. The detectors also determine the beam momentum and trajectories into the target at the few mr level, and count the number of π , μ , and e beam particles. The system we propose to use to accomplish these tasks includes GEM chambers and scintillating-fiber (SciFi) arrays as detectors, with a custom FPGA system to count the beam particles and supply beam PID information to the trigger.

1. SciFi Detectors

We plan to use sci-fi detectors with 2-mm circular fibers at both IFP and target locations. These detectors would provide crude position information and ns-level time resolution for identifying beam particles and their momentum. We expect to readout the SciFi arrays with multi-anode PMTs, which should provide resolution no worse than 1 ns.

The beam momentum (and an RF time) will be determined at the intermediate focal point in the channel. With the dispersion at the focus of 7 cm/%, the position only needs to be determined to a few mm. Coupled with the requirement of a 10 - 15 MHz rate of beam particles – recall that the flux is higher at the IFP than at the target – we use a fast sci-fi array. Based on the test run measurements, we will construct a remote adjustable collimator with thin scintillating fibers at the edges to reduce edge scattering. The plan is to cut the acceptance in the dispersive direction to reduce the flux, generally a narrower momentum distribution of the beam particles. The detector, behind the collimator, will have two planes, each with 96 2-mm fibers 5-cm high - to match the beam profile at the IFP. The distributions at the IFP are fairly flat, so each fiber will see only a modest rate of about 0.1 - 0.15 MHz. Light guides attached to the short fibers will bring the light to the maPMTs.

Within any RF bucket there is a 20% - 30% chance of a second particle and a 0.2% - 0.3% chance the second particle is in the same fiber, but only a 10% chance of a second particle that also reaches the target. When two particles are in the same RF bucket and the same fiber, the beam PID and trigger systems will only be aware of the earlier one. Elsewhere we have argued that we will suppress events where there appears to be a π at the IFP and target SciFi detectors. However, there is no reason to do so at the trigger level if there two e 's, two μ 's, or one of each. Each of these event types can potentially be analyzed, and we will argue later that the particle momentum does not need to be determined on an event by event basis.

The 10 - 15 MHz IFP singles rate quoted above includes an estimated 5 MHz of neutron rate. Since the neutron background at the IFP is spread out in RF time, neutron hits could appear to the beam PID system to be π 's, μ 's, or e 's. We plan to reduce our sensitivity to this background by requiring a coincidence between the two IFP SciFi planes. While this reduces our efficiency for charged particles somewhat, it does not effect the cross section extraction, as we also use the SciFi to count the number of beam particles.

The target SciFi array provides a second RF time measurement that improves the performance of the hardware beam PID system. The SciFi array will consist of 3 planes of 2-mm circular fibers in an XYU configuration, for higher efficiency along with some redundancy. Our plan is to instrument a region of about 5-cm diameter, so each SciFi plane will consist of about 25 5-cm long

fibers. With a 5 MHz rate at the target, there is a 10% chance of a two particles in any RF bucket, and a $\approx 1\%$ chance that the two particles are in the same fiber in any of the planes.

The target SciFi array also improves our ability to analyze event data with second tracks. With a 5 MHz rate assuming the GEM integrates over a 100 ns time, there is a background GEM track in 50% of the events. The SciFi array determines the position of each event to within a few mm^2 region out of a few hundred mm^2 beam spot, which allows the two tracks to be separated with $>99\%$ efficiency if they are in different RF buckets. Some events with two particles in the same RF bucket can be analyzed; for here we just note that if we ignore these events, the consequent 10% reduction in the statistics should make little difference.

2. GEM Detectors

The GEM chambers have resolution $< 0.1 \text{ mm}$ (σ) and rate capability of tens of MHz/cm^2 with pixel readout. Although Monte Carlo studies indicate that multiple events through the chambers 30-50 ns apart can be resolved; for here we assume that the GEM chamber readout will integrate over all tracks within a $\approx 100 \text{ ns}$ window.

At low rates, 2 GEM chambers 10 cm apart determine the trajectory into the target on an event by event basis to $\approx \sqrt{2} \times 0.1/100 = \sqrt{2} \text{ mr}$, better than is needed, as it is less than the multiple scattering from the GEM chamber.

At high rates, random background trajectories lead to problems. Consider two particles going through two chambers at nearly the same times, giving hits at two positions in each chamber. How does one know which hit in chamber 1 is associated with which hit in chamber 2 - which are the two real tracks and which are the two “ghost” tracks? With 5 MHz rates there are second tracks in 50% of the events within the 100 ns GEM time constant. Having a third chamber generally eliminates the ghost tracks, as the position of the track in the 3rd chamber is determined at the few mm level, limited by multiple scattering, as compared to the few cm size of the beam.

Hampton University has built a set of six GEM chambers currently operated as two tracking telescopes in the OLYMPUS experiment at DESY. The OLYMPUS experiment aims to compare the elastic electron-proton and positron-proton cross sections with high precision to determine the effect of two-photon exchange. The OLYMPUS GEM telescopes consist of three GEM elements each and are used to detect small-angle elastic lepton scattering for the purpose of luminosity monitoring. The OLYMPUS GEMs are very suitable to be used as beam GEM chambers for this proposed experiment. The detectors have been performing very reliably and stably, with achieved spatial resolutions around $70 \mu\text{m}$ and efficiencies close to 100%. The FPGA controlled readout is based on the APV25 frontend chip, and a mature software package has been developed to read out the raw data, to identify and locate charge clusters, to subtract pedestals and to eliminate common-mode noise, to form hit locations, and to carry out track fitting. As OLYMPUS data taking is expected to be completed by January 2013 followed by final calibration and survey activities, these detectors including their readout electronics become available for MUSE in the first half of 2013. It is envisioned to transfer the GEM telescopes to PSI in spring 2013. In a first application, they will be used to determine beam properties such as the beam size and divergence at the πM1 channel in a further test experiment planned for May/June 2013. Further, UVa has two existing GEM chambers available that are consistent with our requirements. The small GEM chambers are relatively inexpensive, costing only of the order of \$10,000, so it is relatively inexpensive to construct additional chambers if needed.

3. Beam PID System

Our proposed system needs to separate the different particle types by RF time at the hardware level to suppress pions and to allow the beam flux for each particle type to be determined. We have started the conceptual design of an FPGA-based scaler + beam PID system. It would take RF signal and scintillator inputs and provide distinct output signals for each of the 3 beam particle

types to be used as input to the trigger. We demonstrated in the Technical Design Report that such a system can provide $\approx 99\%$ efficiency at detecting μ 's and e 's while suppressing triggers from π 's by a factor of 10^5 . Counting the beam PID system signals determines the appropriate beam flux directly. We plan to subdivide the 20-ns beam period into 16 time channels, each of width about 1.25 ns, so that as a scaler we would measure counts vs. RF time. Although the electron RF time is independent of momentum, the π and μ times are not, so the module needs programmable windows to use for the different particles as a function of beam momentum.

The beam particle identification system relies solely on RF timing. At the analysis level one also has available time of flight between the IFP and target SciFi detectors. At 210 MeV/ c the e , μ and π time of flight differences are 3 - 7 ns, similar to the separation in RF time. Thus time of flight provides an extra method of PID with a similar quality of particle identification as the RF time. At lower momenta, the time of flight differences are greater, enhancing the ability to distinguish between particles.

Although we cannot demonstrate a need for a higher resolution timing system for beam PID, it is clear that a higher resolution system would make the analysis clearer and easier. As a result we have started looking into a quartz Cerenkov detector to add to the beam line equipment. By orienting the quartz at the Cerenkov angle and reading out the light with a multi-channel plate, tests detectors have obtained 200 ps resolution [27]. Such a detector would improve RF time and time of flight to the spectrometer scintillators, for use at the analysis level in background rejection. For the 115 MeV/ c setting, π 's do not give signals in this detector as β_π is too small, but we do not plan on changing the Cerenkov radiator for higher momenta; our intent is to use this as a timing detector rather than as a Cerenkov PID detector. Also note that the SciFi detectors could not simply be replaced by quartz Cerenkov detectors, since it is necessary to detect the π 's so that accidental coincidences with the π 's can be vetoed.

4. Beam Monitor Detectors

While the GEM detectors provide a monitor of the beam position stability, unbiased with the accidental coincidence background trajectories in the event data, the SciFi's do not have time resolution needed to precisely monitor the time stability and thus the momentum of the beam. To accomplish this task, we intend to mount a set of high-precision scintillators downstream of the target in the beam line, directly monitoring the beam flux and RF time, and time and momentum stability. Essentially this is the same technique that we already used in the beam test measurements, except that the scintillators will not be in the position with the optimal time separation of the particle types for the momenta we are running.

The South Carolina scintillator design requires that we keep rates in each scintillator at the MHz level or below for optimal timing. This requires that the scintillators be moved a few meters downstream of the target, and that several paddles are used so that the rate is not too high in any one paddle. This setup is shown in cartoon form in Fig. 15. The scintillators will be read out as part of the normal event data, so we will actually be monitoring an unbiased distribution of accidentally coincident particles that did not trigger the DAQ.

D. Target

Two common techniques for hydrogen targets are the use of liquid hydrogen targets and the use of hydrogen in a plastic, such as CH₂ or scintillator, along with a carbon target for background subtraction. The main concerns related to the target are multiple scattering and energy loss, which limit the possible target thickness.

Because of the sharp drop of the cross section with angle, multiple scattering, primarily in the target, affects the measured cross section. An estimate of this effect is shown in Fig. 10. The effect is insensitive to energy, with large sensitivity at forward angles due to the sharp drop of the Mott cross section with angle near 0° . For forward angles the multiple scattering needs to

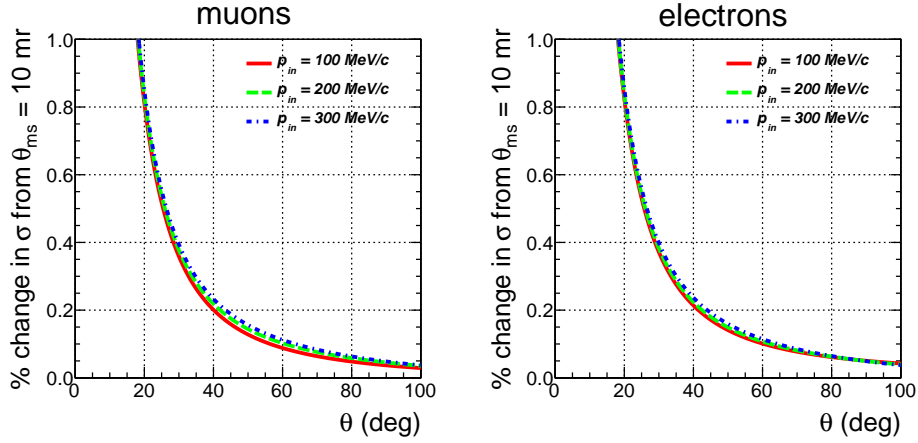


FIG. 10. Effect of multiple scattering on measured cross sections for muons (left) and electrons (right). The increasing systematic uncertainty at small angles from multiple scattering is one of several reasons cross section measurements will be limited to about $20^\circ < \theta < 100^\circ$.

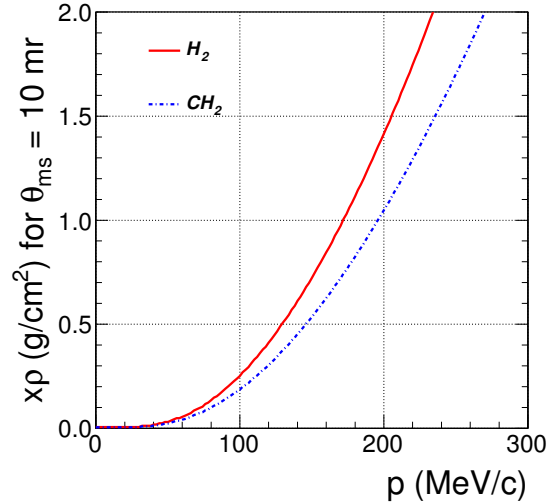


FIG. 11. Thickness of CH_2 or liquid hydrogen targets leading to 10 mr multiple scattering, as a function of momentum.

be limited to several mr, or the cross sections need to be corrected for this effect; we adopt both approaches. Keeping multiple scattering small particularly limits the target thickness for the 115 MeV/c setting, to about 0.3 g/cm^2 . One can see from Fig. 11 that the target will have about 10 times more hydrogen in it for equivalent multiple scattering effect if cryogenic hydrogen is used rather than CH_2 , which makes liquid hydrogen the preferred target, as it reduces the needed beam time by an order of magnitude. Since multiple scattering can be reasonably well estimated, it is possible to unfold the multiple scattering from the measured cross sections to determine the form factors.

Because of energy loss in the target, the beam momentum changes as the beam passes through

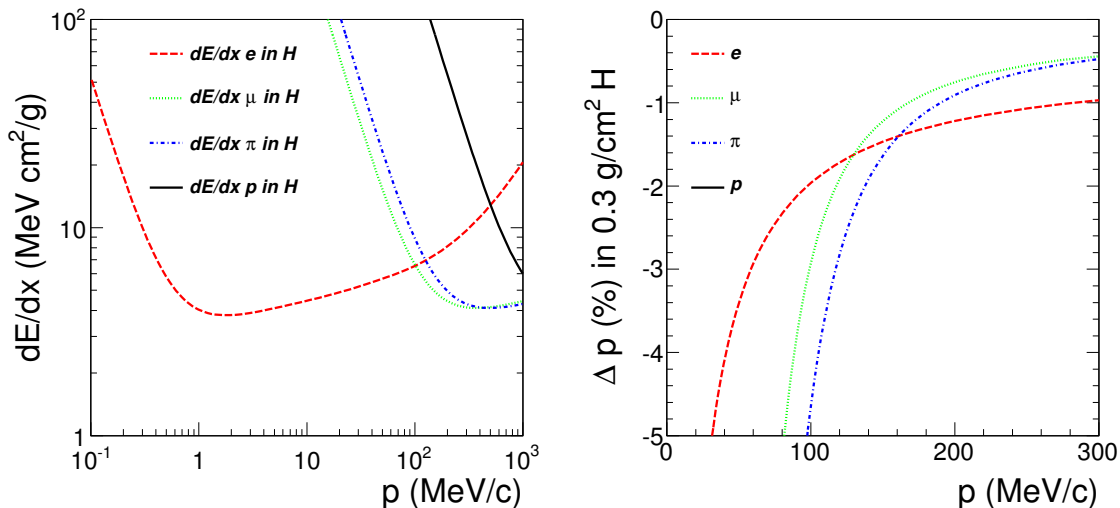


FIG. 12. Left: dE/dx in hydrogen. Right: Change in momentum for particles passing through a 0.3 g/cm² hydrogen target. Protons lose a large fraction of their energy and are off scale.

the target. Figure 12 shows dE/dx for the π 's, μ 's and e 's in the beam, along with the energy loss for these particles passing through a target of thickness 0.3 g/cm². The energy losses were taken from NIST ESTAR [28] for the electrons and NIST PSTAR [29] for protons. For μ 's and π 's, dE/dx was set to the proton dE/dx at the same $\beta\gamma$. For μ 's in the momentum range of interest the momentum drop is about 1% – 2%, much larger than our required momentum knowledge of $\approx 0.1\%$, but not a problem based on the estimates of averaging over the beam momentum shown in Fig. 7, since the energy loss and the average interaction momentum can be calculated reliably. For a foil target, the correction relies entirely on the calculated energy loss. For a liquid hydrogen target, a 0.3 g/cm² target is about 4 cm long, and the interaction position can be determined to about 1 mm. This will allow the energy loss correction as a function of distance and energy loss to be studied, providing a valuable cross check.

At present, there does not appear to be an available LH₂ target at PSI. A low-luminosity target with basically the needed functionality has recently been constructed by the Michigan and Maryland groups for use in the Fermilab E906 Drell-Yan experiment. This target could not simply be moved to PSI as the target cells are much longer than desired for a low energy μp experiment. But it provides a guide to the scale of effort and funding needed to construct a similar system from scratch for PSI: about 2 person-years of effort and US \$300,000 [30].

A particular concern with cryogenic targets, in particular those whose scattering chambers are built with thin windows (as the our design will be) is the freezing of background vapor contaminants on the cold surfaces of the targets. This can lead to enhanced energy loss and multiple scattering. We plan to mitigate the effect by designing the target area in a way which will contain several cold baffles (at LN₂ temperature) with large surface area, located so as to be invisible to the detectors, which will reduce the fraction of contaminants adsorbed on the target. In addition, these baffles will reduce the heat load on the target generated by blackbody radiation.

To summarize, a cryogenic target, about 4 cm long, maximizes the hydrogen thickness consistent with the needed systematic uncertainties at the lowest beam momentum setting. A second longer cell can be used for higher momentum settings. Given the greater desirability but larger cost and longer time to construct an LH₂ target vs CH₂ and C foil targets, we plan to use the foil targets for the initial set of test measurements, until an LH₂ target is ready for operation.

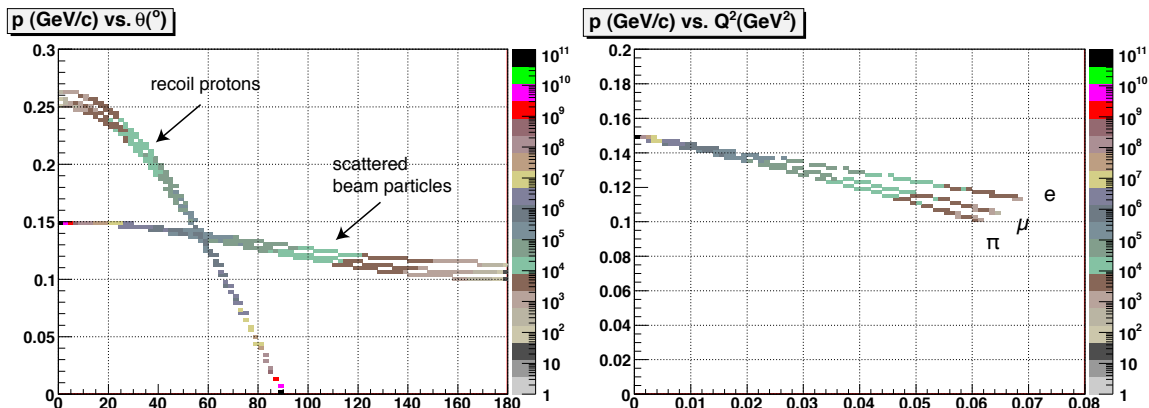


FIG. 13. Left: Curves of p vs θ_{lab} for elastic scattering of 150 MeV/ c π 's, μ 's, and e 's from protons. With very similar kinematics and at this resolution the lines are overlapping and largely indistinguishable. The recoil proton lines reach from about 0.25 GeV/ c at $\theta = 0^\circ$ out to 90° , while the scattered beam particles only vary from about 0.15 GeV/ c to 0.1 GeV/ c . At larger angles the differences of $p_e > p_\mu > p_\pi$ can be seen. The differences in the recoil protons near 0° can also be seen. Right: curves of p vs. Q^2 for elastic scattering of 150 MeV/ c π 's, μ 's, and e 's from protons. The upper curve is for e 's and the lower curve is for π 's. The recoil protons are not shown.

E. Scattered-Particle Detectors

1. Overview

The detector system needs to have a well determined solid angle and well determined central angles, although measurements on an event by event basis only need to be at the few mr level. We need to cleanly identify and trigger on scattered μ 's and e 's to determine their cross sections, and identify but not trigger on π 's. We now focus on what the scattered-particle distributions will be.

When a low-energy beam of π 's, μ 's, and e 's impinges in an idealized experiment upon a proton target, no inelastic processes are kinematically allowed, so only elastic scattering and some processes included in radiative corrections are possible, up to pion production threshold – corrections to this picture are discussed below. Pion production threshold occurs at beam momenta of about 250 MeV/ c for μ 's, so only processes in the radiative corrections are present. For e 's, pion production becomes kinematically possible at 150 MeV/ c , but the cross section is basically negligible until beam energy is much higher and one starts to climb up the low-energy tail of the Δ resonance. These processes are present in simulations, but are basically not a concern for most of the energy range discussed here, and we do not consider them further.

This idealized situation is reflected in Fig. 13, which shows the kinematics for scattering on protons. The kinematics for the scattered particle and for the recoiling proton are similar for all beam particles. The momenta of scattered π 's, μ 's, and e 's change slowly with angle, and are similar at the same angle. The recoiling proton momentum exceeds the beam momentum at forward angles, and drops to 0 by 90° – the proton cannot be scattered backward of 90° .

One complication to the simple picture is that the beam also interacts with the atomic electrons. The heavy μ 's and π 's scatter from the atomic electrons, losing energy, undergoing multiple scattering, and producing knockout electrons or δ rays. Figure 14 shows that the heavy beam particles when interacting with atomic electrons basically multiple scatter and go forward with little change in their momentum vector, while producing low momentum, few MeV/ c electrons that go out over a range of angles. Because the μ 's and π 's go forward, they do not lead to triggers, and are not a concern. The beam positrons (electrons) undergo Bhabha (Moller) scattering with the atomic electrons, producing high momentum particles for small angles, forward of about 15° , but only few

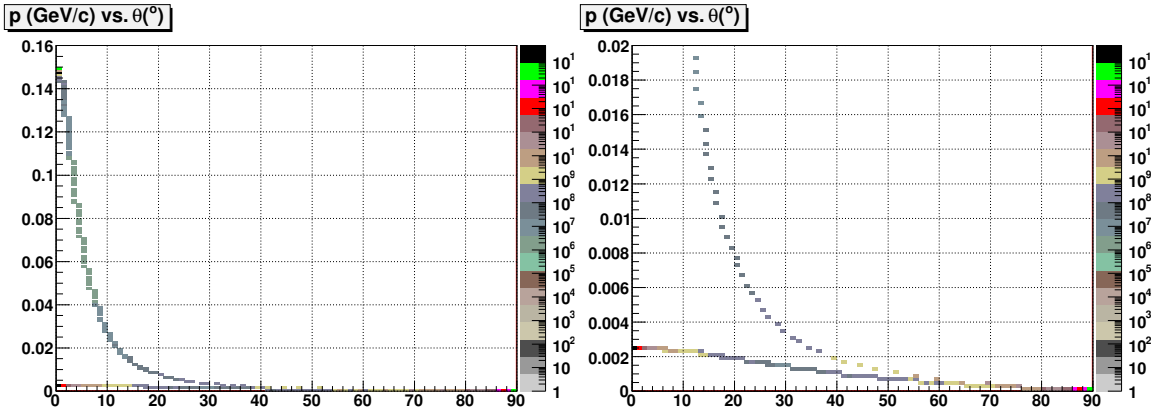


FIG. 14. Scattering of 150 MeV/c π 's, μ 's, and e 's from atomic electrons. The panels are the same, except the vertical scale is expanded for the right panel. For π 's and μ 's, the much heavier beam particle goes forward at nearly the beam momentum, while the recoil electron goes out over a range of angles at very low momentum, a few MeV/c. For an incident e^+ (e^-), there is Bhabha (Moller) scattering, leading to electrons with 10 MeV/c or larger up to about 15° .

MeV/c particles for larger angles. The high rate of higher momentum e 's in the forward direction are another reason why we limit our planned angle range to about $20^\circ < \theta < 100^\circ$. Note that one background of concern in the simulations is Moller / Bhabha scattering in the upstream detectors.

A second complication to the simple picture is radiative corrections, which are discussed further in Sec IV I. Here we consider the Bremsstrahlung part of the radiative corrections, which leads to real photons. In the peaking approximation, an electron can radiate a photon in the beam direction before scattering, or in the scattered direction after scattering. The result of these processes is to remove electron flux from the beam or scattered electrons from being detected, so that the actual “Born” cross section is different from the experimentally measured cross section. This part of the radiative correction is already present in GEANT simulations, where the correction leads to electron distributions with long tails toward lower momentum, but muon distributions with very short tails.

The detector system in the range of about $20^\circ < \theta < 100^\circ$ will have similar rates of e 's and μ 's that scatter from protons, with momenta similar to the beam momenta. We need to track, identify, and generate triggers from these particles. There will also be a large rate of low momentum, < 10 MeV/c electrons from scattering from atomic electrons in the target that should not generate triggers. Finally, there will be a small rate of recoil protons that escape from the target into the region of the detectors; the rate of these protons is sufficiently small that we neglect further consideration of them.

The rate of Moller (or Bhabha) scattering off electrons in the target is a potential concern. However, the cross section peaks for particles either going forward out of the range of our detectors, or going out at $\theta_{lab} \approx 90^\circ$ with very low momentum, so that they do not generate triggers. The GEANT simulations indicate that the major issue with Moller (or Bhabha) scattering is with scattering off upstream detectors, which can lead to triggers, although at the analysis level these will not track back to the target.

Multiple scattering in the target is a significant effect, limiting the angle reconstruction to ≈ 10 mr. The correction to the cross section arising from the 10 mr multiple scattering is small enough that it can be corrected for reliably, but we need to ensure that the total resolution does not become significantly larger. Thus, it is necessary to minimize additional multiple scattering by having the wire chambers as the first detector element and by ensuring that the wire chamber trajectory resolution is well below the intrinsic 10 mr limit. While on an event by event basis the trajectory only needs to be determined to a few mr resolution so that the chamber resolution does

not significantly add to the multiple scattering, the chamber positioning must be precise enough that the scattering angle offsets are below 1 mr.

In summary:

- Detectors cover an angular range of about $20^\circ - 100^\circ$. The forward angle is limited by considerations of high rates and increasingly difficult systematic uncertainties. The largest angle covered is limited by the lack of scattering rate at large angles. To obtain excellent statistics, we are also aiming for an azimuthal coverage of 50% of 2π .
- Good angle resolution requires the initial detector stack element to be a wire chamber. Background singles rate are small.
- Efficient triggering will be provided with the thick scintillators; GEANT simulations show efficiencies well above 99%, except in the case of e^+ .
- Due to the lack of inelastic processes at lower energy, combined with manageable background rates, we find that there is little benefit from using a magnetic field to either momentum analyze scattered particles or to shield the detectors from the high rate of low-energy electrons. Not having a magnetic field should simplify the “optics” of the experiment and make precise cross sections easier.

Precise cross section measurements are traditionally done with small solid angle detectors, adjusting their angle and using luminosity monitors to help determine relative normalizations. This is the technique used in the Mainz ep experiment. While we are confident that such a technique would work here, the low luminosity makes the measurement of a range of angles prohibitive time-wise. We will instead construct and precisely position large solid angle detectors with the needed systematic precision.

2. Spectrometer Detectors

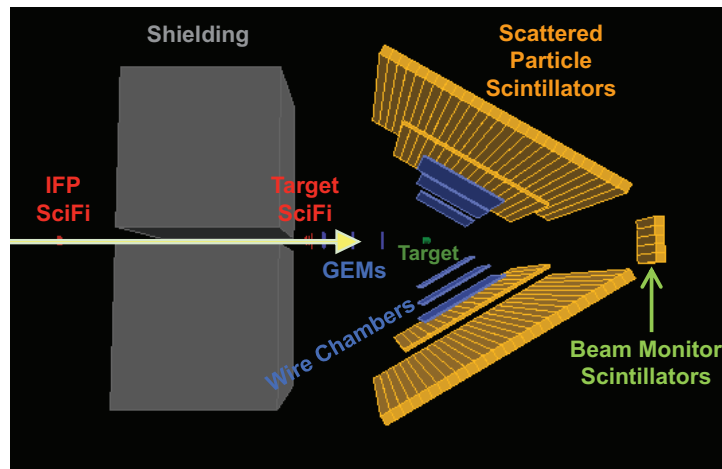


FIG. 15. A cartoon of the experimental setup.

Our plan for the experimental configuration is shown in Fig. 15. The “spectrometer” for the scattered particles consists of wire chambers and trigger scintillators.

As indicated above, rates are small in the wire chambers. The GEANT simulations give a singles rate in the chambers in both spectrometer arms combined of up to 150 kHz. For a conventional wire chamber with ≈ 100 ns drift times, this rate leads to background tracks in about 1.5% of the events. Half of these are in the wrong spectrometer arm, and the redundancy available with multiple chamber planes and scintillator paddles should allow essentially all background tracks to be eliminated.

The key issue with the beam and scattered particle chambers is being able to know the geometry of the chambers and position them so that scattering angle offsets can be determined to better than 1 mr. We will keep the placement of wire chambers in a compact design around the target, with a support structure machined so that the wire chambers are all positioned to about $10 \mu\text{m}$ over distances of several tens of cm, so that in principle angle offsets are below $100 \mu\text{r}$. This relies on a similar precision in the construction of the chambers. To confirm the precision, the table will be constructed so that it can be rotated with an angular precision of better than 0.1 mr, allowing the chambers to be put in the beam directly behind the GEM chambers, and oriented relative to them.

The wire chambers for the proposed experiment at PSI will consist of three chambers on each side of the beam line, and the design will be based on the Jefferson Lab Hall A Bigbite wire chambers [31, 32] as shown in Fig. 16. Each wire chamber will contain six wire planes divided into three groups: U , U' , V , V' , and X , X' wires oriented at $+30^\circ$, -30° , and 0° , respectively, with respect to the horizontal direction. Each chamber plane will consist of alternating sense and field wires spaced 5 mm apart, with parallel planes offset by 5 mm. Shifting the second plane by half of the wire spacing helps to remove the left-right ambiguity in the track reconstruction, while having wires in three orientations helps both to remove ambiguities in the case of multiple tracks and to determine a track even if a wire is inefficient in a given plane.

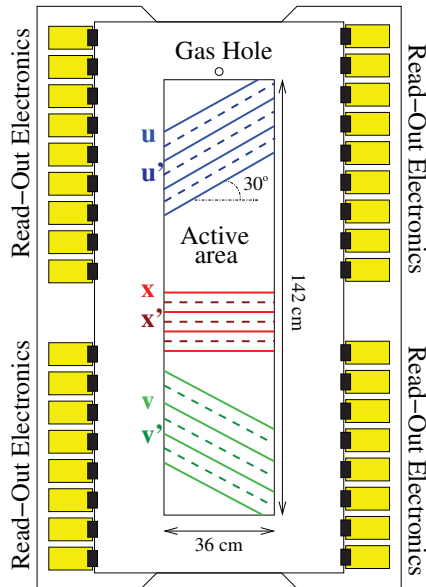


FIG. 16. Schematics of the front BigBite wire chamber indicating the orientation of the wire planes with respect to the horizontal direction.

The location from the pivot and the sizes of the chambers are listed in Table III along with the number of wires per chamber. The spacing between the chambers will be about 10 cm from the front of one chamber to the back of the next chamber. Assuming a resolution of $100 \mu\text{m}$ and having the center of the front and back chambers spread out over a 20 cm distance will provide about a 0.7 mr angle determination, which is ultimately limited on an event-by-event basis by multiple

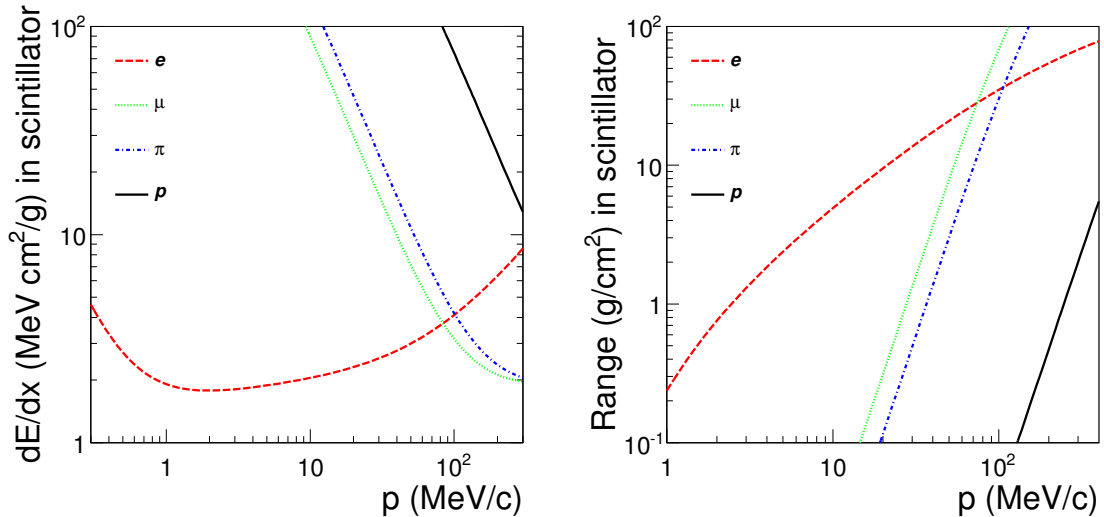


FIG. 17. Left: dE/dx in scintillator. Right: Range of particles in scintillator.

scattering.

TABLE III. Wire chamber parameters including the distance from the pivot, chamber active area and the number of wires.

Chamber	Distance (cm)	Active Area (cm ²)	Number of wires per chamber
Front	25	50 × 45	346
Middle	35	70 × 60	480
Back	45	90 × 80	616

Scattered particle scintillators provide triggering, RF time determination, and particle identification. The scintillators will be the outermost elements in the detector stack. Positioning scintillator bars from 50 to 73 cm from the target requires bars that are about 1.0 - 1.6 m long. We plan two scintillator layers on each side of the beamline to allow a loose, highly efficient trigger. The layers will consist of 17 to 27 paddles. The back layer will have a slightly increased angular coverage compared to the front plane to ensure high trigger efficiency even when particles scatter in the front plane. Note that the scintillators do not need to be positioned with the same accuracy of the chambers, and an independent less-precise support system can be used for them. An overview of the design parameters for the scintillators is given in Table IV.

TABLE IV. Design parameters for the scintillator walls.

	Front wall	Back wall
Number of scintillator bars	17	27
Scintillator cross section	6 cm × 2 cm	6 cm × 6 cm
Scintillator length	103 cm	163 cm
Target to front-face distance	50 cm	73 cm

Important considerations for the scintillator paddles are energy loss of the particles passing

through them and timing. Figure 17 shows dE/dx in polystyrene scintillator calculated from NIST ESTAR [28] for the electrons and NIST PSTAR [29] for protons. For pions and muons, we take dE/dx to be the same as for protons at the same $\beta\gamma$. Except for protons, all particles in the $\approx 100 - 200$ MeV/ c range of interest are close to minimum ionizing. Because dE/dx increases with momentum for the electrons but decreases with momentum for the π 's and μ 's, it might be possible to use energy loss at the analysis level for some indication of particle type, but this will be difficult as fluctuations in dE/dx are large. In the test run measurements with 5-cm thick scintillators we were able in some settings to see multiple, but always overlapping, peaks in the scintillator charge (QDC) spectra. Figure 17 also shows that the < 3 MeV/ c electrons present over much of the angle range stop in 1 g/cm² of scintillator, which is in the first layer of a multilayer scintillator trigger. Stopping 10 MeV/ c Moller or Bhabha electrons requires about 4 cm of scintillator. At this point it does not appear that there is any benefit to adding in an absorber for the forward angles, 20° - 30°, where these electrons appear, but we will study the issue further.

The second key feature of the scintillators is precise timing. The South Carolina group has recently built scintillators 6 cm \times 6 cm by up to 2 m long for the Hall B / CLAS 12-GeV upgrade project. These scintillators have 56 ps (σ) resolution, at the analysis level rather than in hardware, with shorter bars having better resolution. The RF time determined by the scattered particle scintillators is then entirely limited by the ≈ 400 ps width of the RF time peaks due mainly to the width of the proton beam. Thus scattered particle types are separated by about 4 ns / 400 ps = 10 σ at the analysis level. Thus, given such paddles and fast TDCs, in the analysis particle identification based on time of flight is sufficient in itself. RF timing of the scattered particles provides much more than adequate particle identification by itself. This assumes particles reconstructing as scattering from the target, as backgrounds can have different path lengths to the detectors. The several ns variation in timing as light propagates along a 1.0 - 1.6 m long scintillator paddle prevents determination of a useful RF time at the trigger level from these scintillators.

To summarize, the needed angular precision and resolution can be achieved with precise positioning of conventional wire chambers. Trigger scintillators can provide high efficiency for triggering and precise RF timing, more than sufficient for particle identification at the analysis level.

F. Backgrounds

1. Pion and Muon Decays

The beam μ 's and π 's are unstable particles with lifetimes of ≈ 2.2 μ s and 26 ns, respectively, which decay in flight. The decays can lead to background and triggers from particles that do not substantially interact with beam line elements.

As an example, the decay of 150 MeV/ c π 's leads to a decay cone of 120 MeV/ c μ 's at angle of about 14° from the pion direction. With $\beta_\pi \approx 0.75$, about 11% of the π 's will decay every meter. Any of the π 's that decay after or just before the target SciFi detector will still give a signal in that detector that indicates a π beam particle. This π signal will prevent triggers, thus these π 's are not an issue. The main possible concern is whether π 's can decay just upstream of the SciFi detector, miss it, and go into the detectors causing backgrounds. We plan to prevent this by having a shielding wall just before the SciFi array, with the SciFi covering the aperture in the shielding wall. While the final design has not yet been worked out, a tungsten collimator is likely.

Muon decays are more of an issue. For 150 MeV/ c μ 's, $\beta_\mu \approx 0.8$, only about 0.1% of the muons decay per meter of flight path. The decay electrons typically come out in a cone at about 35° relative to the μ direction with a momentum of about 90 MeV/ c , but the distribution is broad as this is a three-body decay. Muon decays lead to two corrections in the cross section determination:

- The first correction is that the flux of muons through the target is not the same as the flux of muons counted in the beam sci-fi arrays. This is a $\approx 0.1\%$ correction that affects the absolute normalization.

- The second correction is that about 0.1% of the scattered μ 's decay as they travel to and pass through the detector stack.

Both corrections are small, and ultimately will be done using a GEANT simulation that includes the detector geometry.

The biggest problem with muon decays is that at the trigger level decays in flight are not too different from muon scattering events. About 0.004% of the muons in the beam decay in the target, but this leads for positive polarity at 150 MeV/c to a trigger rate of about of 24 Hz. Actually, at the trigger level muons decaying anywhere near the target can reach the detectors and look like scattering events, so in fact the DAQ rate from muon decays will be a few hundred Hz. This should be compared with the estimated 3 Hz rate of actual muon elastic scattering from the target. At the analysis level most of the decay muon events are easily eliminated as they do not track back to the target. Since z -target resolution depends on the angle, the decay muons are more easily removed at large-angles. The actual rate of decay muons can be directly calculated, but will be measured as well during the empty target runs. We are left with about an order of magnitude more decay muons than elastic scattering muons. At forward angles, the statistical uncertainties in each bin are about 0.1%, but the fluctuations in the decay muon rate will increase the uncertainty to about 0.3% when the muon decay background is subtracted.

While these statistical uncertainties are adequate, as they are smaller than the point-to-point systematic uncertainties, we are interested in improving the rejection of electrons. There are three possibilities: dE/dx in the scintillators, a Cerenkov detector in the detector stack, and time of flight. Here we focus on time of flight. Since the electrons from muon decays have $\beta = 1$ they arrive at the spectrometer scintillators about 0.7 ns earlier than do scattered muons. This is not in itself sufficient for separating the events as we found in the test run that the muon RF time distribution is 400 - 500 ps wide. Instead we would need to upgrade the timing available from the target SciFi detector. A recent development [27] used quartz Cerenkovs oriented at the Cerenkov angle and read out through a multichannel plate to provide 200 ps resolution. The muon decay background is one of our motivations for deciding to employ this technology, with an additional beam line detector just upstream of the target SciFi.

2. Cosmic Rays

The total rate of e 's or μ 's in the beam ranges from 1 \rightarrow 5 MHz in our proposed kinematic settings. Thus, if there is a cosmic ray that can generate a trigger, there is a 2 \rightarrow 10% chance that it is coincident with a beam e 's or μ . A detector the size of ours will have a cosmic rate of about 600 Hz, reduced to about 150 Hz of apparent scintillator triggers, reduced by the random coincidences with beam e 's or μ 's to a readout rate of about 15 Hz or less. At the analysis level these events do not generate tracks back to the target, and will be rejected. The distributions of scintillator times for cosmic events are also very different from the distributions of scattered particle events. The probability of cosmic backgrounds during an actual event is small, about 10^{-5} ; this is too low a level to affect cross sections.

3. End Cap Scattering

Scattering from the target end caps leads to a background that cannot be removed at the trigger level. In general the only way to remove this backgrounds is to measure them and subtract, which can be done with a fit to the data. At the analysis level, the end caps lead to peaks in reconstructed z -target about 1-mm wide at large scattering angles, but about 1 cm wide at forward angles. Thus, target fiducial cuts can be used to reduce these backgrounds, but only at larger angles. However, care must be taken in doing this for comparison of electron to muon cross sections, as the electrons have less multiple scattering leading to a slightly narrower end cap peak.

Generally the end cap background is significantly less of a problem than is μ decays. Although we are at small Q^2 , the nuclear form factor falls significantly, and the rate of end cap scattering

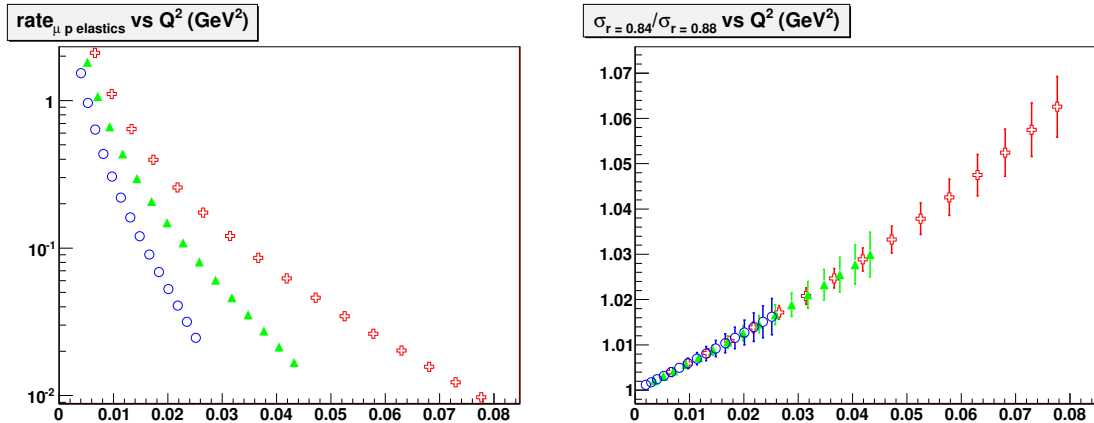


FIG. 18. Left: estimated count rates for μp elastic scattering for the conditions described in the text. Squares are for the 210 MeV/c data, triangles are for the 153 MeV/c data, and circles are for the 115 MeV/c data. Right: Projected cross sections with uncertainties for 30 day runs at each beam momentum. Points are the same as in left panel. For simplicity, we show the data all lying on the curve expected if the form factor is linear and reflects an rms radius of 0.84 fm, divided by the similar projection for a radius of 0.88 fm. Note that since the form factor ratio is taken to be linear, the cross section ratio is quadratic. But the approximation that $G_E = 1 - Q^2 r^2/6$ starts to fail in the Mainz data around 0.02 GeV², as shown in Fig. 3.

is about three times smaller than the rate of scattering from hydrogen. This is also due to the thinness of the end caps in the beam.

4. Scattering from Upstream Detectors

The thickness of the upstream detectors leads to a significant scattering rate from them. These events are easily removed at the analysis level. The main issue is if they generate too many triggers for the DAQ to handle. In our GEANT simulations, the rate of such events was typically at the level of 2 kHz, which is not a problem. However, the rate depends on details of the beam distributions, our detector geometry, and any collimation that we construct; thus we will continue to pay attention to this issue as we continue our test measurements and detailed experimental designs.

G. Rates

We calculated μp elastic scattering rates with several assumptions. The Kelly form factor parameterization [17] was used. We used the beam fluxes shown in Table I, with the constraint that we will limit the channel acceptance so that the flux at the target is no more than 5 MHz. The target was assumed to be 0.3 g/cm² of hydrogen. We assume 60 day runs at each setting, and neglect inefficiencies from detectors, triggers, computer dead time, or event analysis. The detectors are assumed to cover 50% of the 2π azimuthal angle range. The scattering angle range is 20° - 100°. This estimate is the same as that in the Technical Design Report, except for our limiting the beam flux to 5 MHz rather than 10 MHz. The resulting elastic scattering rates are typically a few Hz for muons and several times this for electrons due to the higher electron flux. For display we sum the data with 5° bins and plot at the central Q^2 of each bin.

Figure 18 shows the resulting count rates and uncertainties for positive polarity beam at the three incident momenta. The $\mu^+ p$ elastic scattering rates are modest, and require a long run to

bring the level of the uncertainties down towards the levels achieved in the Mainz experiment. The sub-1% statistical uncertainties we are attempting to achieve here are several times better than the typical several percent μp scattering experiments discussed earlier.

The μ^- fluxes are several times smaller than the μ^+ fluxes for the full channel acceptance, but with the limit of 5 MHz rate on target the μ^- fluxes, and thus the estimated rates, range from about $3\times$ smaller to $2\times$ larger than the π^+ rates. We have not yet considered whether to adjust the allocation of time to optimize the uncertainty on the 2γ -exchange extraction.

H. Trigger

The purpose of the trigger is efficiently read out scattered μ 's and e 's in the angle range $20^\circ < \theta < 100^\circ$, while suppressing unwanted backgrounds, especially π induced events. The rate of such triggers is quite modest, at the level of a few tens of Hz, in the presence of much larger backgrounds. The trigger combines the beam particle identification information with a scattered particle scintillator coincidence in identifying events to read out.

As described before, and discussed in the Technical Design Report, the beam PID system is at least 98 - 99% efficient in identifying particles – a small inefficiency is not important as missed events are not counted in the beam normalization, and the readout rate is not greatly impacted. The beam PID system also suppresses π 's at the level of $>10^5$. Thus, normal π scattering events are a small fraction of read out events, and any π scattering events read out can be rejected at the analysis level due to the superior timing available.

For a trigger we require that the beam PID system finds a μ or e and no π in the same RF pulse, and that two spectrometer scintillators fire that approximately point back to the target. Simulations discussed elsewhere indicate that the scintillator coincidence is at least 99% efficient, with the major inefficiency being for e^+ , which can annihilate before firing both scintillator planes. It is important to know the absolute efficiency of the scintillator part of the trigger, as this directly impacts the normalization and shape of the form factors. Because the simulations indicate that the efficiency is high, this should end up being a small systematic uncertainty, once we obtain data to confirm the simulations.

The main issue for the trigger, discussed in more detail in the Technical Design Report [25], is suppressing backgrounds from unwanted events. Examples of these events include:

- π scattering events
- decays in flight of π 's and μ 's leading to μ 's and e 's in the spectrometer that are not from the target
- tails of the beam going through thick walls, leading to a much larger scattering probability
- random coincidences of cosmic- or π -induced events in the spectrometer with beam particles
- scattering of μ 's and e 's from the scattering chamber windows or target endcaps.

Some types of background events can be suppressed at the trigger level, whereas others will be read out, and can only be suppressed at the analysis level.

The following outlines how we will deal with the backgrounds mentioned.

- π scattering events are suppressed by the beam PID
- decays in flight: π decays near or after the target SciFi are suppressed by the beam PID, but μ decays near the target cannot be suppressed at the trigger level. Muon decays in flight work out to be a major background as they will generate a few hundred Hz of triggers; the decay rate of μ 's at these beam momenta is about 10^{-3} per meter. At the analysis level the μ decay events are reduced by requiring tracks from the target region, because the timing in the scintillators is slightly different for scattered μ 's than for $\mu \rightarrow e\nu_\mu\bar{\nu}_e$ ($0.2 \rightarrow 0.8$ ns depending on kinematics), and by differing energy losses in the scintillators, but ultimately

a number of events will have to be calculated from the muon flux, lifetime, and the Monte Carlo to subtract. Note that we directly measure the appropriate muon flux, and the lifetime is known much more precisely than needed, so the uncertainty on this correction is mainly a question of making sure the Monte Carlo is tuned well enough. This rate will also be directly measured in empty target measurements.

- Tails of the beam at the trigger level through collimation and requiring particles to pass through the target beam SciFi. They are suppressed at the analysis level through fiducial cuts on the GEM tracks of the beam particles into the target.
- Random coincidence of cosmics are eliminated at the analysis level through the lack of tracks pointing to the target. Random coincidences of π 's are suppressed at the trigger level by only generating triggers when there is not π within the same RF bucket.
- Scattering from the chamber windows and the target endcaps looks essentially the same at the trigger level as scattering from the hydrogen. At the analysis level, the windows can be removed through tracking reconstructions, but the endcaps cannot be cleanly removed. Determining the rate from the end caps is a standard problem in scattering experiments, and this background is usually suppressed by a combination of dummy target measurements for direct subtraction, and varying z -target cuts, as the resolution changes with angle.

I. Radiative Corrections

Radiative corrections may be considered to consist of two types of processes. Processes including Bremsstrahlung and virtual Compton scattering lead to the emission of real photons, changing the kinematics of events, and leading to tails in particle momenta distributions. Processes including vertex corrections and virtual particle-antiparticle loops change the cross section from what one would expect in the Born approximation – only a single photon is exchanged, with no other photons or particles in the Feynman diagram – but do not change the kinematics.

First, we consider the Bremsstrahlung part of the radiative corrections, which leads to real photons. The electron is light, and is accelerated by the electromagnetic fields of atoms as it passes through a material and scatters from atomic nuclei and electrons, so it, compared to the heavier muon, copiously emits photons. This part of the radiative correction is already present in GEANT simulations, where the correction leads to electron distributions with long tails toward lower momentum, but muon distributions with very short tails. Figure 8 already indicated that the size of (part of) the Bremsstrahlung corrections for muons are quite small. In the simple peaking approximation, electrons radiate photons either in the beam direction before scattering, or in the outgoing direction after scattering. Thus the electron direction is largely unchanged, while its momentum decreases. The Brem correction goes to 0 with decreasing beam momentum as β^2 .

There are several corrections that affect the cross sections without real photons being emitted. Here we focus on the Coulomb correction, which proved important in determining the proton radius in previous analyses. The Coulomb correction varies with angle from about 0% at forward angles to 0.6% (0.8%) at 90° for muons (electrons). It is insensitive to beam energy, with a 1% change in beam energy leading to a 0.5% (relative) change in the correction. The Coulomb corrections go to zero with decreasing beam momentum, proportional to β .

While vertex corrections are reduced for muons as compared to electrons, due to the larger mass, we note that virtual loop corrections are the same for muon and electron scattering, as the loop is an e^+e^- pair in either case due to the lighter mass of the pair; the beam flavor is unimportant.

At the kinematics of this measurement, the radiative correction for electrons, $\sigma_{Born} = \sigma_{experiment}/(1 - \delta)$, is typically about $1 - \delta_e \approx 85\%$ – the Born cross section is about 15% larger than the experimental measurement; the Brem correction is largest, and as a consequence the muon radiative corrections are significantly smaller.

An important but perhaps difficult part of the radiative corrections are the two-photon exchange corrections. There are now a number of experiments studying these corrections due to the interest

in firmly reconciling the cross section and polarization transfer measurements of the proton electric form factor. The corrections have been studied experimentally for many years, but never with sufficient precision. For this experiment, the important thing to note is that the two-photon exchange corrections are expected to be small and will be directly measured through the comparison of $\mu^\pm p$ scattering and similarly of $e^\pm p$ scattering. An estimate of the size of the corrections can be seen in Fig. 19, taken from [33], which compares several two-photon exchange calculations. The important points to note are that for each Q^2 the range of calculations is small, and the corrections are generally small at high ϵ , equivalent to forward angles.

J. Systematic Uncertainties

TABLE V. Estimated experimental systematics for μp elastic scattering. Systematics for ep scattering are similar. For systematics that vary with angle, a typical value for $\theta = 50^\circ$ is given.

Systematic Uncertainty	Point-to-point (%)
Scintillator efficiency	0.1
Wire chamber efficiency	0.1
Trigger efficiency	0.1
Beam momentum	0.1
Averaging over beam momenta	0.1
Knowledge of angle	0.3
Multiple scattering	0.3
Solid angle	0.1
Radiative correction	0.5
Cell wall subtraction	small
Cosmic ray subtraction	small
π / μ decay corrections	small
TOTAL	0.7

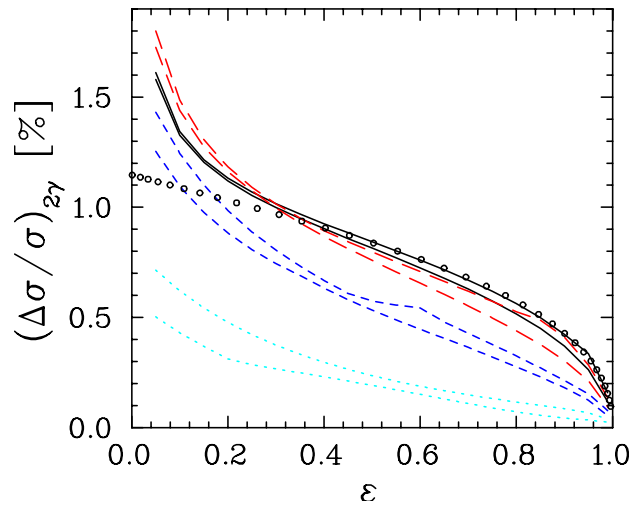


FIG. 19. Comparison of several two-photon exchange calculations. Solid, long-dashed, short-dashed, and dotted lines show the range for $Q^2=0.01, 0.03, 0.1,$ and 0.2 GeV^2 , respectively. See [33] for details.

The systematic uncertainties have largely been discussed above, and are summarized and estimated in Table V. Here we only consider the point-to-point uncertainty, as the data will have to be renormalized with a fit, as we are unable to have absolute normalizations at the tenths of a percent level. Thus certain systematics, such as the target thickness, essentially vanish and are not considered. (In reality the target thickness comes in at a small level as it induces energy loss and multiple scattering, but the magnitude of the uncertainty is hard to estimate without studying how well the GEANT simulation compares with the data.)

The systematics with the biggest uncertainties concern the knowledge of angles. Since there is no strong magnetic field used to momentum analyze particles in the detector system, knowledge of angles largely comes down to an issue of mechanical design, so that wire chambers are precisely constructed and positioned, and a calibration scheme to determine the position of the wire chambers. The chamber wire positions can be measured with a precision traveling microscope, and the chamber position can be determined using a precision rotary table with the chambers rotated a known angle so beam goes through both the GEM chambers and the wire chambers. The systematics related to the multiple scattering averaging over angle, shown in Fig. 11, can be reduced by correcting for this effect; the correction relies on knowing material thicknesses to calculate the multiple scattering, but is insensitive to the form factors as the effect arises largely from the Mott cross section.

The best check of systematic uncertainties is the measurement and overlap of a large number of data points. To that end we have proposed three beam energies at which both e 's and μ 's can be measured. The π M1 beam line would allow additional momenta for μ 's, near 130 MeV/ c , but there is no other momentum at which the e 's are well separated that is significantly different from the three selected. This situation leads us to plan an additional full statistics point at which the wire chambers and scintillators are rotated a few degrees while the beam momentum setting is held constant, as a pure check of several aspects of the experimental systematics.

Note that if we are comparing cross sections of one reaction to cross sections of another at the same angle, then systematics like the effect of angle offsets or multiple scattering largely cancel, as they are similar for μ 's and e 's of both polarities.

The background subtraction entries in Table V are listed as small, as the dominant uncertainty from these subtractions comes in as a statistical, rather than a systematic, uncertainty.

K. Cross Section and Radius Comparisons

The first goal of the experiment is to directly compare the μp and ep cross sections measured. The statistical uncertainties of the cross sections range from about 0.3 to 1% at the larger angles. The systematic uncertainties discussed above are at about the 0.5% level. Because absolute uncertainties are larger, the data sets will be fit with a form factor parameterization that includes the $Q^2 = 0$ constraints, to determine the absolute normalization of each independent data set.

The first comparison to make is to check for the size of two-photon exchange effects by comparing the “+” and “-” cross sections. While the point-to-point uncertainties might be at the several tenths of a percent level, these effects largely are the same for “+” and “-” cross sections and thus largely cancel in the ratio. Coulomb corrections are an exception, since they are opposite for the + vs. - charges. The resulting uncertainty will then be dominated by statistics, and will be about 0.5% at small angle to 1.5% at large angles. Since the two-photon exchange effect should vary smoothly with Q^2 at each beam momentum, as shown in Fig 19, the remaining fluctuations are not as important as the average trend of the data.

The average of the “+” and “-” data then provides the cross section with the two-photon exchange effects entirely removed, since that are equal but opposite in sign for the two beam polarities. At this point the μp and ep cross sections can be compared. Because of the different masses, Q^2 is slightly different for the two reactions at the same beam momentum and angle, but the point-to-point corrections still largely cancel. Angle offset corrections, for example, as shown in Fig. 9, vary by about 1% across the full angle range, but differ by $<0.1\%$ for angles a few degrees apart. As a result, the comparison of μ to e will have slightly larger systematics but slightly smaller

statistical uncertainties than do the two-photon exchange comparisons.

It is important to note here a point not otherwise discussed in this proposal: because the muon is massive and not fully relativistic ($\beta_\mu = 0.74 \rightarrow 0.89$), the cross section formula for μp includes terms not present in the usual expression given for $\beta = 1$, essentially massless ($m_e/M_p \ll 1$) electrons. This leads to the μp cross section being as much as about 4 times larger than the ep cross section [34]. The formulas are exact, so there is no uncertainty associated with this correction.

Comparison of the form factors is more precise than comparison of cross sections; as the cross sections depend on the form factors squared, the relative uncertainty on the electric form factors is half the relative uncertainty on the cross sections, allowing the μ and e determined proton form factors to be compared at the few tenths of a percent level. Since the magnetic form factor only makes a small contribution to the cross section, its uncertainty is larger.

The fits that determine the form factors and the normalizations will also determine the slopes of the form factors at $Q^2 = 0$, the proton radius. For the radius the variation in Q^2 is important, so there is not the cancellation in systematic uncertainties discussed above. Here we present only the results; a more extensive discussion can be found in the Technical Design Report Section XVI. The uncertainty in the radii separately determined with μ^-p or μ^+p or e^-p or e^+p are nearly the same, around 0.01 fm, as the systematic uncertainties are somewhat larger than the statistical uncertainties. One can improve on the comparison by, for example, only allowing the linear, radius term in the fit to vary between the μp and ep data sets. This leads to a relative measurement of the radius at the 0.006 fm level, to be compared with the current ≈ 0.036 fm discrepancy.

V. COLLABORATION RESPONSIBILITIES AND COMMITMENTS NEEDED FROM PSI

The MUSE collaboration is comprised primarily of people with experience in electron scattering experiments. Many members of the collaboration have worked together for periods exceeding a decade. Many of the younger members of the collaboration have previously worked with older members of the collaboration during their time in graduate school or as postdocs.

The collaboration members generally work on experiments which last several years, with beam times ranging from about a month up to 1 or 2 years. The usual commitment of a collaboration member at any point in time is to several experiments, one or two under analysis, one or two running or about to run, and one or two being developed for running in a couple years. Each member typically plays a leading role in one or two experiments and a supporting role in others.

The core of the collaboration at present can be viewed as the institutions taking a commitment to develop major parts of the experiment and/or obtain funding and/or have Ph.D. students and postdocs essentially fully committed to the experiment. A summary of commitments to the basic equipment development and other tasks is shown in Table V. In addition, we are expecting Ph.D. students and / or postdocs focused on the experiment from GW, Hebrew University, MIT, Rutgers, and Tel Aviv; these people will spend much of their time on site at PSI.

Because of the need to construct new equipment, it will be necessary to submit funding proposals for the experiment. Three proposals have been submitted or are being prepared. Prof. E. Piasetzky (Tel Aviv) submitted a proposal to the Binational Science Foundation in October 2012 which would fund a student for four years plus travel; Profs. W. Bertozzi (MIT), S. Gilad (MIT), R. Gilman (Rutgers), and J. Lichtenstadt (Tel Aviv) are coPIs. Prof. G. Ron (Hebrew University) submitted a proposal (“CHARMS: CHARGE Radius via Muon Scattering”) for an ERC starting grant in October 2012 which would provide the cryogenic target for this experiment and the beam Cerenkov counter. Prof. R. Gilman has submitted to Rutgers for internal review a pre-proposal for an NSF MRI grant, which would cover the other equipment needed for the experiment: electronics, trigger, scintillators, SciFI’s, and wire chambers. If approved by Rutgers, this proposal would go to NSF in February 2013.

Once approved, the collaboration plans on an outgoing series of short (month long) test runs in the $\pi M1$ beam line, intended to study the beam line, develop and test the equipment, and validate the simulations. In parallel with this activity the collaboration will be obtaining funding

Device	Institution	Person
π M1 Channel	PSI	K. Dieters
Scintillating Fibers	Tel Aviv	E. Piasezky
Scintillating Fibers	St. Mary's	A. Sarty
GEM chambers (existing)	Hampton	M. Kohl
Beam Cerenkov Counter	Hebrew University	G. Ron (Co-Spokesperson)
Cryogenic Target System	Hebrew University	G. Ron (Co-Spokesperson)
wire chambers	M.I.T.	S. Gilad
Scintillators	South Carolina	S. Strauch
Electronics and Trigger	Rutgers	R. Gilman (Spokesperson)
Readout Electronics and DAQ System	George Washington	E. J. Downie (Co-Spokesperson)
Radiative Corrections	George Washington	A. Afanasev
Analysis and Radius Extraction	Argonne	J. Arrington

and constructing equipment. Equipment can be ready about 2 years after funding is obtained.

As the equipment is constructed, installation in the π M1 area and basic commissioning of the experiment will likely require about 6 months. Some of the components can be tested separately. Once the experimental equipment is ready, we desire a one month test run followed by a several month analysis period, followed by a one year production run. We would prefer basically exclusive access to the π M1 area during the period from the start of installation to the completion of the production run, though small low current tests should not be a problem.

The commitments needed from PSI are standard for experiments. They include:

- approval of the experiment
- infrastructure support: access to the π M1 area, office space, access to power and computer networks
- about 1 month of test runs per year
- minor adjustments to the π M1 channel: installation of NMR or Hall probes to monitor dipole stability, minor adjustments to vacuum pipes in the downstream half of the beam line, addition of a concrete shielding wall just before the detectors
- engineering / design coordination, to ensure the equipment is consistent with laboratory requirements
- installation support

VI. SAFETY ISSUES

The proposed experiment makes use of detectors and targets that are common to subatomic physics experiments. At this point we do not have a detailed system design, so we only briefly review common safety issues for these systems. We do not consider beam-related safety concerns as the π M1 area and its safety systems have been operational for many years.

Cryotarget: Standard low power cryotargets involve several liters of liquid hydrogen at a temperature of about 20 K in a cell with thin walls, typically encased in a vacuum system. The main potential issue is a rupture of the cell and vacuum system. Rupture of a vacuum system can generate a loud sound that can damage hearing; warning signs, roped off areas, and ear protection for those who must work near the system are a standard counter measures. If the target ruptures the hydrogen liquid expands in volume about three orders of magnitude and quickly rises through the air. This presents potential oxygen deficiency hazards and potential damage to exposed skin

or eyes. We believe that the size of the building containing the π M1 area and the quick rise of the lighter than air hydrogen mitigate any potential ODH hazard. Damage to skin and eyes is limited by protective clothing including eye protection.

Low Current, High Voltage: Wire chambers and phototubes operate with few kV DC power, which could if shorted provide a power source to ignite a fire or harm a person either directly or through surprise and an ensuing accident. All HV is shielded so that it cannot be directly accessed, and supplied by power supplies with trip limits set, so that any shorting of the supply leads to the supply turning off.

High Current, Low Voltage: Numerous electronics modules require power supplied at low voltage, perhaps 5 V, but at large currents, often many hundreds of amps for the entire experiment. Chamber mounted readout electronics are one example of this; electronics modules mounted in VME or NIM crates are another example. Because of the high current capabilities, shorts to ground might lead to exploding wires, fires, or personal injury if, e.g., the short is through jewelry worn by a person. Standard safety techniques include having no exposed contacts and fuses.

Chamber Gas: Wire chambers are operated with various gas mixtures typically supplied from high pressure gas cylinders. There are well established gas cylinder safety procedures since in accidents gas cylinders can quickly become very effective missiles. The ODH hazard is minimal as it is unlikely that a large amount of gas would be released into a small part of the M1 area. A more common concern is that many gas mixtures are in principle flammable if sufficiently concentrated with the oxygen in air, and must be kept from an ignition source, such as a spark of flame. It is common in this case to analyze for the area the maximal leak rate permitted for the chamber systems, and monitor system leak rates. In the case of the π M1 area, it is likely that the chamber gas use is so small given the building containing the area that even venting the used chamber gas directly into the area does not cause a flammable gas hazard. The GEM chambers have been operated in the past with a non-flammable mixture, 70% Argon and 30% CO₂, but we have not at this time specified the gas mix for the chambers for tracking scattered particles.

Mechanical Issues: The detector systems are heavy in total and require properly designed and constructed support structures. Assembly of the apparatus is likely to require a crane; there are standard safety procedures for crane use. Accessing some of the higher detector elements might involve use of a ladder or platform, which might further lead to fall protection issues. Again, there are well developed safety procedures in these cases that must be designed into the system constructed.

VII. TECHNICAL REVIEW COMMENTS

An initial version of the technical review document was prepared in June 2012 for a technical review of MUSE, R-12-01.1, held at the Paul Scherrer Institut July 25, 2012. A copy of the Technical Design Report can be found at [25]. The review subcommittee had several questions and comments, which are repeated and addressed here. Several of the questions are discussed in more detail in an updated technical design report.

The committee thinks there is a very strong physics case for the proposal. A particular strength of the proposal is the ability to study μ^\pm and e^\pm scattering within the same experiment. The experiment has the potential to provide critical data towards the solution of the so-called proton radius puzzle.

We agree with this assessment.

The committee felt that the TDR in its current form is not suitable to serve as a basis for a conclusive decision about the proposal. However, the committee was pleased to note that much useful information that was missing in the TDR has been added in the presentations.

Certain aspects of the TDR were undergoing rapid advances at the time of its original writing, particularly the simulations and the wire chamber design. We have upgraded the TDR to reflect developments since it was originally submitted.

The crucial point is to establish if the beam properties allow the proposed measurements to be made, as was pointed out by the BVR committee in its 43rd session in February 2012. To this end

a detailed understanding and study of the beam through measurements, possibly complemented by simulations, is indispensable. These tests should take place in the autumn of 2012. The beam time for these test has already been approved.

The beam tests should provide essential input and will be a prerequisite for a more complete proposal. It will give the collaboration a much better idea about the amount and nature of the effort that is required.

We agree with the assessment that confirming the beam properties are sufficient for the experiment is crucial. The beam tests and their analysis are ongoing at the time of this writing. The planned beam tests were discussed in the original TDR in Section XVII. The results available at present are presented separately, in Section IV A.

Apart from the beam tests, a full realistic simulation of all aspects of the experiment should be done, paying particular attention to multiple scattering effects and energy losses in material in the beam.

While we have continued to upgrade the simulations, a full realistic simulation is impossible at this time. There are several reasons for this including:

- The beam tune has not been fully re-established
- The beam tune as it exists will not be fully characterized until we run with beam GEM chambers, which we expect to do in May-June, 2013.
- To validate the simulations, we need to run additional tests measuring more directly the effects of multiple scattering and energy loss in detector materials than we have done so far. These additional measurements are planned using two sets of GEM chambers for May-June, 2013.
- We have found in simulations to date that backgrounds are sensitive to design details. While the simulations thus provide guidance, what we consider a full realistic simulation cannot be done without at least an engineering design for the experiment.
- Our current Geant4 simulation code is not optimized and full simulations require extensive computer time. Presently, our simulations use a 12 processor machine to generate 10^7 events in about 10^4 s to study various issues. For the present, we think this is fine, and we plan to do more extensive simulations as the exact beam and detector geometry become better understood. However, if a *full* simulation of the experiment requires matching the planned statistics, using 10^{14} beam particles, it is clearly not easily done, as it requires of order 1000 machines of the type we have running for 1 year.

Nevertheless, we have confidence from our existing simulations and systematics estimates that the multiple scattering and energy loss issues can be handled adequately.

The committee raised a number of further questions/issues the collaboration should address:

1. to provide a detailed plan for the available manpower during beam tests and operations, taking into account possible delays beyond 2016.

The collaboration is composed of a number of institutions that are commonly involved in experiments requiring beamtime in the range of 1 month – 2 years. In none of them have detailed plans for manpower during operations been made this far in advance of the run time, before the equipment has even been funded. It is impossible to know at this point the schedule of MUSE or of possible other competing experiments – collaboration members are involved in efforts at other laboratories such as Jefferson Lab, Fermilab and Mainz – that might run about the same time. Having sufficient staff available to run a particular experiment is a common issue that all of these experiments deal with, and having to support two experiments at once is an issue that has at times happened to many of the experiment groups in the MUSE collaboration.

With respect to manpower at PSI, the plan can be divided into two basic stages, the initial testing / commissioning stage, and the data production phase. Operations during the initial phases generally require experts to be present to install, test, commission, and debug their parts of the experiment. Operations during the data production phase are more routine, can be partially

run remotely, particularly as certain problems can be resolved remotely, and experts need more to be available than to be present.

The initial test run included colleagues from Tel Aviv working on the SciFi's, from GW, Hebrew U, MIT, and Weizmann working on the DAQ, from Rutgers working on analysis, from PSI working on the beamline, and only one person, from Argonne, providing general support. A few other colleagues were interested in taking part but ultimately the scheduling did not work out.

For the measurements planned for May-June 2013, we expect most of the 2012 group of people to return, with the major additional contribution being people from Hampton U for the GEM chambers.

As equipment is constructed and brought on site, people from the responsible institutions will need to be onsite. Our most recent experience with such an effort with a similar scale to this is probably E906 at Fermilab, which is about twice the size of this experiment in terms of cost or people. For E906 there was a core group of about 5 - 10 people regularly on site for a period of about 1.5 years putting the experiment together. This included local staff as well as students, postdocs, and faculty on sabbatical. We envision a roughly 2 year period where we will need to have a similar size and composition group based at PSI for the experiment. However, due to the cost of living in Switzerland and certain issues with paying for travel, it is likely that people from some institutions will cycle to and from PSI for one month periods.

For the experiment itself, the shift commitment will likely be about 4 - 5 weeks of shifts per person over the course of the production run. This is similar in magnitude to other medium / high energy scattering experiments. Usually we would expect to have a group of several grad students and postdocs on site at any one time for analysis and problem solving, plus a group of 6 people to run shifts. It might be possible to take advantage of computer networks and experts on site and allow one person on each shift doing online analysis to run some of their shifts remotely; we have taken a portion of the test data this way.

2. how to deal with the fact that the beam structure is not sharp in time.

As discussed in the beam test report [24], the width in time of the beam particles is about 500 ps (σ). This is not an issue for the RF time determination in hardware, where we expect to have detectors with resolution of ≈ 1 ns (σ) and an FPGA system with 1.25 ns binning determining the particle type. It should also not be an issue for the event analysis, where we will have the time of flight between the IFP and target SciFi arrays as well.

3. timing of experiment and monitoring of stability

We interpret the committee's remarks here to indicate concern with the RF time determination for the experiment.

We plan to use high precision scintillators directly sampling the beam downstream of the target to monitor the combined stability of the channel setting and proton beam position / timing stability. The electron portion of the spectrum is sensitive mainly to the primary proton beam properties, while the π and μ spectra are also affected by changes in the channel momentum. We expect to separately monitor the channel magnets in slow controls.

4. should there be some effort to try to improve the IFP timing?

The ability to reject π 's and separate e 's and μ 's is discussed in the Technical Design Report, section IV. There we conclude that the use of SciFi arrays with 1 ns timing (σ) is sufficient both for hardware triggering and data analysis. The time of flight differences shown in Table II are of similar size to the RF time differences at 210 MeV/c, but are much greater at 115 MeV/c, and provide an additional method of beam particle identification.

To date, we have been unable to convince ourselves improved timing over what we can get from IFP and beam SciFi's with maPMTs is absolutely needed, though clearly it is very desirable and would make the analysis cleaner. We have found that a relatively simple, inexpensive technology has been tested [27] that can provide an improved timing measurement. The technology uses a quartz Cerenkov radiator mounted at the Cerenkov angle relative to the beam, so that some of the Cerenkov photons emitted go directly into a multi-channel plate. The tested system obtained 200 ps (σ) timing. As described elsewhere in this proposal, we now intend to implement a quartz Cerenkov detector in the experiment, and funding for it has been requested.

5. to what accuracy does the event-by-event momentum need to be known

We plan to measure the momentum on an event-by-event basis for fine tuning RF time and time of flight cuts, and for determining the beam momentum distribution for input to our Monte Carlo simulations. But at this point we do not believe this momentum determination is actually needed on an event-by-event basis for determining the cross sections. As discussed in relation to Figure 7, the experiment is actually quite insensitive to the beam momentum. Beam momentum offsets act largely like normalization errors similar in size to the offsets. We have checked that the sensitivity to momentum offsets scales with the momentum offset as shown in Figure 7 up to offsets of at least a few percent. Energy loss in the detectors will lead to a broader distribution in momentum, but averaging over a beam momentum distribution is a smaller effect than beam momentum offsets.

6. what is the influence of the average beam momentum error?

This is shown in Figure 7.

7. to provide an error estimate of effects due to the target walls

This was discussed in the technical report in Section XIII.A.3, where we proposed measuring and subtracting the background. We plan to run with a dummy target with target walls 6 times thicker than for the actual LH2 target. The statistical error on the subtraction is optimized if 25% of the beam time is devoted to the dummy run, and 75% to the LH₂ run. In this case the statistical uncertainty is 40% greater than it would be for a target consisting entirely of LH₂ with no walls.

The walls also increase multiple scattering slightly over what a wall-less target would have, but we assume the comment is not directed to this effect.

8. to provide an estimate of theoretical uncertainties of radiative correction calculations

This will be provided by Andrei and Edith and John.

9. how important is it to have data for the lowest (115 MeV) energy?

For purposes of directly comparing cross sections or form factors from the various probes and kinematic settings, or comparing our data to the Mainz data, the 115 MeV/c setting does not add much to the experiment. For extraction of the radius however, because the lowest beam momentum setting goes to lower Q^2 , we estimate that it yields a radius about equal in uncertainty to the upper two momentum settings combined. Thus it reduces the uncertainty in the radius by about a factor of square root of two.

Perhaps more importantly, in some models of physics beyond the standard model, there can be new light particles that only affect the extractions of the form factors – at this point presumably only in the case of muons – at the lowest Q^2 , so it is desirable to measure to the lowest Q^2 possible.

Also important in our view is that the lowest momentum gives us a third point of overlap in the experiment when we compare the different momentum settings. It is a common but unfortunate problem that when one compares different parts of a measurement of the same quantity that the subset points often do not overlap as well one expects. One can see examples of this in small parts of the Mainz data set; we have encountered it in many other experiments. We do not know whether such problems will occur for MUSE, but we do know from past experience that having more settings is generally helpful in trying to sort out these problems. A large number of energy settings is common in electron scattering experiments, and we think it is fair to say that everyone with electron scattering experience would prefer more beam momentum settings, not a reduction to two.

Thus, we think it is a mistake at this time to limit the number of beam momentum settings to two.

10. is there a bias on angle resolution and cross section measurements due to large multiple scattering?

The effects of multiple scattering presented in our simple estimates are based on the usual Gaussian approximation - the GEANT simulations are more realistic. In our simple estimate, the tails are underestimated by a few percent. This leads to the effects of multiple scattering on the cross sections being underestimated by several percent, since there is a larger effect from large angle scattering than from small angle scattering. The analysis of the experiment and corrections will of course be based on the GEANT simulations.

The committee is looking forward to receive a complete TDR. If the feasibility of the experiment can be demonstrated and the points mentioned above have been addressed in a satisfactory way, the committee will seriously consider a positive recommendation.

A revised version of the TDR is expected to be available about one week after this proposal is submitted.

VIII. SUMMARY

No resolution to the proton radius puzzle has been found. The puzzle has attracted widespread interest. We repeat the quote from the Jefferson Lab PAC: “*Testing of this result is among the most timely and important measurements in physics.*”

We propose to measure μ^\pm and e^\pm elastic scattering, at the same time with the same equipment, which allows

- the highest precision scattering experiment determination of the consistency of the μp interaction with the ep interaction
- a test of the importance of 2γ exchange effects
- a determination of the radius from the data sets, to check its consistency

The experiment is technically feasible on a time scale of about 3 - 4 years. It requires under \$2M in equipment funding. We are requesting about two additional months of test runs, a 6 month installation and commissioning period, a 2 month dress rehearsal run, and a 12 month production run.

-
- [1] R. Pohl, A. Antognini, F. Nez, F. D. Amaro, F. Biraben, *et al.*, *Nature* **466**, 213 (2010)
- [2] P. J. Mohr, B. N. Taylor, and D. B. Newell, *Rev.Mod.Phys.* **80**, 633 (2008), arXiv:0801.0028 [physics.atom-ph]
- [3] I. Sick, *Phys.Lett.* **B576**, 62 (2003), arXiv:nucl-ex/0310008 [nucl-ex]
- [4] P. J. Mohr, B. N. Taylor, and D. B. Newell, (2012), arXiv:1203.5425 [physics.atom-ph]
- [5] J. Bernauer *et al.* (A1 Collaboration), *Phys.Rev.Lett.* **105**, 242001 (2010), arXiv:1007.5076 [nucl-ex]
- [6] X. Zhan, K. Allada, D. Armstrong, J. Arrington, W. Bertozzi, *et al.*, *Phys.Lett.* **B705**, 59 (2011), arXiv:1102.0318 [nucl-ex]
- [7] C. Carlson, to be published.
- [8] R. Pohl, K. Pachucki, G.A. Miller, and R. Gilman, to be published.
- [9] R. Pohl *et al.*, Workshop on the Proton Radius Puzzle at the Trento European Center for Theory in Nuclear Physics and Related Areas, [http://www.mpg.mpg.de/~rnp/wiki/pmwiki.php/Main/WorkshopTrento.emShut Stop](http://www.mpg.mpg.de/~rnp/wiki/pmwiki.php/Main/WorkshopTrento.emShut%20Stop)
- [10] B. Batell, D. McKeen, and M. Pospelov, *Phys.Rev.Lett.* **107**, 011803 (2011), arXiv:1103.0721 [hep-ph]
- [11] A. Gasparian *et al.*, Jefferson Lab PAC38 proposal PR-11-1xx, unpublished.
- [12] L. Cardman, J. Lightbody Jr., S. Penner, S. Fivozinsky, X. Maruyama, W. Trower, and S. Williamson, *Phys.Lett.* **B91**, 203 (1980)
- [13] E. Offermann, L. Cardman, C. de Jager, H. Miska, C. de Vries, *et al.*, *Phys.Rev.* **C44**, 1096 (1991)
- [14] L. Schaller *et al.*, *Nucl.Phys.A* **379**, 523 (1982)
- [15] W. Ruckstuhl, B. Aas, W. Beer, I. Beltrami, K. Bos, *et al.*, *Nucl.Phys.* **A430**, 685 (1984)
- [16] R. Ellsworth, A. Melissinos, J. Tinlot, H. Von Briesen, T. Yamanouchi, *et al.*, *Phys.Rev.* **165**, 1449 (1968)
- [17] J. Kelly, *Phys.Rev.* **C70**, 068202 (2004)
- [18] L. Camilleri, J. Christenson, M. Kramer, L. Lederman, Y. Nagashima, *et al.*, *Phys.Rev.Lett.* **23**, 153 (1969)
- [19] I. Kostoulas, A. Entenberg, H. Jostlein, A. Melissinos, L. Lederman, *et al.*, *Phys.Rev.Lett.* **32**, 489 (1974)
- [20] A. Entenberg, H. Jostlein, I. Kostoulas, A. Melissinos, L. Lederman, *et al.*, *Phys.Rev.Lett.* **32**, 486 (1974)
- [21] L. Camilleri, J. Christenson, M. Kramer, L. Lederman, Y. Nagashima, *et al.*, *Phys.Rev.Lett.* **23**, 149 (1969)

- [22] V. Tvaskis, J. Arrington, M. Christy, R. Ent, C. Keppel, *et al.*, Phys.Rev. **C73**, 025206 (2006), arXiv:nucl-ex/0511021 [nucl-ex]
- [23] J. Arrington *et al.*, “A Measurement of Two-Photon Exchange in Unpolarized Elastic Electron-Proton Scattering,” Jefferson Lab experiment 05-017.
- [24] W. Briscoe *et al.*, “MUSE Test Run Report,” Unpublished, http://www.physics.rutgers.edu/~rgilman/elasticmup/testrun_report.pdf.
- [25] A. Afanasev *et al.*, unpublished, http://www.physics.rutgers.edu/~rgilman/elasticmup/mup-prop_finals.pdf.
- [26] http://aea.web.psi.ch/beam2lines/beam_pim1.html.
- [27] M. Albrow, H. Kim, S. Los, E. Ramberg, A. Ronzhin, *et al.*, JINST **7**, P10027 (2012), arXiv:1207.7248 [physics.ins-det]
- [28] ESTAR program, <http://physics.nist.gov/PhysRefData/Star/Text/ESTAR.html>.
- [29] PSTAR program, <http://physics.nist.gov/PhysRefData/Star/Text/PSTAR.html>.
- [30] W. Lorenzon, private communication.
- [31] N. Liyanage, “Commissioning of Tracking Package for Bigbite Spectrometer,” unpublished, 2012.
- [32] M. Mihovilovic, K. Allada, B. Anderson, J. Annand, T. Averett, *et al.*, Nucl.Instrum.Meth. **686**, 20 (2012), arXiv:1201.1442 [nucl-ex]
- [33] J. Arrington, (2012), arXiv:1210.2677 [nucl-ex]
- [34] E. Borie, (2012), arXiv:1207.6651 [physics.gen-ph]